



UCLouvain

Institute of Mechanics,
Materials and Civil Engineering

Robust optimisation of the pathway towards a sustainable whole-energy system

A hierarchical multi-objective
reinforcement-learning based approach

Doctoral dissertation presented by

Xavier RIXHON

in partial fulfillment of the requirements for
the degree of Doctor in Engineering Sciences

December 2023

Thesis committee

Pr. Francesco CONTINO (supervisor, UCLouvain)

Pr. Hervé JEANMART (supervisor, UCLouvain)

Dr. Stefano MORET (ETH Zurich)

Pr. Sylvain QUOILIN (ULiège)

© 2023
Xavier Rixhon
All Rights Reserved

Contents

Symbols	iii
1 Methodology: Through a variety of complementary tools	1
1.1 Whole-energy system transition model optimisation: EnergyScope Pathway	3
1.1.1 Perfect foresight: One global optimisation of the transition	4
1.1.2 Myopic: Sequential optimisation of the transition with limited foresight	7
1.2 Uncertainty quantification	11
1.2.1 Uncertainty characterisation	11
1.2.2 Polynomial Chaos Expansion	13
1.2.3 Preliminary screening and selection	17
1.3 Agent-based reinforcement learning for energy transition support	17
1.3.1 Reinforcement learning fundamentals and application to energy systems	18
1.3.2 Problem formulation and algorithm	19
1.4 Robustness assessment via PCA	22
1.4.1 Principal Component Analysis: General concept	23
1.4.2 Principal components of the transition	25
2 Robustness assessment of pathway roadmaps	33
2.1 Definition of the principal components of the transition	34
2.1.1 Principal components of each representative year	35
Bibliography	37
A Pathway optimisation under uncertainties	43
A.1 Total transition cost	43

A.2 Imported renewable electrofuels	45
A.3 Installed capacities	47

Symbols

Acronyms

API	application programming interface
BECCS	bioenergy with carbon capture and storage
BEMS	building energy management system
BEV	battery electric vehicle
BTX	benzene, toluene and xylene
CAPEX	capital expenditure
CCGT	combined cycle gas turbine
CCS	carbon capture and storage
CHP	combined heat and power
CNG	compressed natural gas
DC	direct current
DHN	district heating network
DNN	deep neural network
DRL	deep reinforcement learning
ESOMs	energy system optimisation models
EnergyScope TD	EnergyScope Typical Days
EUD	end-use demand
FC	fuel cell
FEC	final energy consumed
GDP	gross domestic product
GHG	greenhouse gases
GSA	global sensitivity analysis
GWP	global warming potential
HP	heat pump
HT	high-temperature

HVC	high value chemicals
IAMs	integrated assessment models
ICE	internal combustion engine
IEA	International Energy Agency
IPCC	intergovernmental panel on climate change
IQR	interquatile range
LCA	life cycle assessment
LCOE	levelised cost of energy
LFO	light fuel oil
LOO	leave-one-out
LP	linear programming
LPG	liquefied petroleum gas
LT	low-temperature
MDP	Markov decision process
MMSA	Methanol Market Services Asia
MTBE	methyl tert-butyl ether
MTO	methanol-to-olefins
NED	non-energy demand
NG	fossil gas
NN	neural network
NRE	non-renewable energy
NSC	naphtha steam cracker
OPEX	operational expenditure
PC	principal component
PCs	principal components
PCA	Principal Component Analysis
PCE	Polynomial Chaos Expansion
PDF	probability density function
PV	photovoltaic
RE	renewable energy
RL	reinforcement learning
SAC	Soft Actor Critic
SDGs	Sustainable Development Goals
SMR	small modular reactor
SVD	singular value decomposition
UQ	uncertainty quantification
VRES	variable renewable energy sources

List of publications

Limpens, G., **Rixhon, X.**, Contino, F., & Jeanmart, H. (2024). “*EnergyScope Pathway: An open-source model to optimise the energy transition pathways of a regional whole-energy system.*” In Applied Energy, (Vol. 358). URL: <https://doi.org/10.1016/j.apenergy.2023.122501>

Rixhon, X., Limpens, G., Coppitters, D., Jeanmart, H.,& Contino, F.(2022). “*The role of electrofuels under uncertainties for the Belgian energy transition.*” In Energies (Vol. 14). URL: <https://doi.org/10.3390/en14134027>

Rixhon, X., Tonelli, D., Colla, M., Verleysen, K., Limpens, G., Jeanmart, H. ,& Contino, F.(2022). “*Integration of non-energy among the end-use demands of bottom-up whole-energy system models.*” In Frontiers in Energy Research, Sec. Process and Energy Systems Engineering, (Vol. 10). URL: <https://doi.org/10.3389/fenrg.2022.904777>

Rixhon, X., Colla, M., Tonelli, D., Verleysen, K., Limpens, G., Jeanmart, H., & Contino, F.(2021). “*Comprehensive integration of the non-energy demand within a whole-energy system: Towards a defossilisation of the chemical industry in Belgium.*” In proceedings of ECOS 2021 conference (Vol. 34, p. 154).

Rixhon, X., Limpens, G., Contino, F., & Jeanmart, H. (2021). “*Taxonomy of the fuels in a whole-energy system.*” In Frontiers in Energy Research, Sec. Sustainable Energy Systems, (Vol. 9). URL: <https://doi.org/10.3389/fenrg.2021.660073>

Limpens, G., Coppitters, D., **Rixhon, X.**, Contino, F., & Jeanmart, H. (2020). “*The impact of uncertainties on the Belgian energy system: application of the Polynomial Chaos Expansion to the EnergyScope model.*” In proceedings of ECOS 2020 conference (Vol. 33, p. 711).

Chapter 1

Methodology: Through a variety of complementary tools

“Technique aussi brûlante que les derniers bilans du GIEC.”
Primero (ft. Romeo), in *Deux deux*, 2022

Assessing the robustness of a whole-energy system transition pathway calls a variety of methodological tools. First and foremost, such an extensive system needs to be represented, i.e. modelled, to further be optimized. This model requires some characteristics to capture the peculiarities of this system such as the intermittency of variable renewable energy sources (VRES), the coupling between the different energy and non-energy sectors and a pathway vision to pave the way from where we are to where we want to go. Then, as looking into the future (i.e. up to 2050 in this work) comes with its lot of uncertainties, these have to be assessed carefully in terms of characterisation and quantification. The former aims at defining the range over which parameters of the model vary. The latter allows assessing the impact that such uncertainties can have on the output of the model. Finally, meeting the environmental objectives while minimizing the cost of the system, accounting for this decision-making process, the uncertainties, and potential shocks/crisis, require therefore a framework to assess the relevance and the timing of the decisions throughout the transition. This work encompasses the optimisation of the policy, i.e. set of actions to take along the transition with a specific methodology to assess its robustness.

Detailing the different tools needed to answer the research questions, this chapter starts with the presentation of the whole-energy system optimization model, EnergyScope Pathway and its myopic formulation. Then, it focuses on the uncertainties,

their characterisation as well as their quantification. Finally, an agent-based reinforcement learning (RL) approach is detailed to address the sequential decision-making process in the uncertain transition with limited vision in the future. The robustness of these policies is assessed via the use of the Principal Component Analysis (PCA).

Contributions

The main methodological contribution of this work is the implementation of the reinforcement learning (RL) approach to simulate and optimize the behaviour of an artificial agent interacting with its environment, i.e. the whole-energy system through its transition. Given the uncertainties and potential shocks of the future, this approach allows the agent to play the transition in a sequential, i.e. myopic, way and optimize the choice and the timing of its actions. This optimization is done through trial and error where the agent repeats the transition with a new set of uncertainties.

Then, to support this step-by-step transition with limited foresight in the future, we have extended the EnergyScope Pathway model [1]. Originally developed to optimize the transition in one global optimisation up to 2050, i.e. perfect foresight, part of this thesis consisted in making this model able to optimize the same transition but with sequential more limited time windows, i.e. myopic approach. Besides its shorter computational time, this approach is more representative an actual decision process with limited foresight in the future [2].

The third principal methodological contribution is the use of Principal Component Analysis (PCA) to assess the robustness of a policy, i.e. how much the optimal pathway is affected by the uncertainties. Given the uncertainties and the timespan of the transition, this approach allows highlighting the main “directions” of variation of the system design (i.e. the installed capacities). After this step of identification, strategies and policies can be projected on these directions to see how robust they are to the overall transition uncertainties.

Finally, more minor methodological developments are part of this thesis. Following an approach similar to Guevara et al. [3], we have extended the ranges of uncertainty developed by Moret et al. [4] to the pathway optimisation. After assessing the relevance of using Polynomial Chaos Expansion (PCE) on the optimisation of a whole-energy system [5], we have applied this uncertainty quantification method on the snapshot model subject to different emission-constraints Rixhon et al. [6] as well as the pathway model. Eventually, starting from the initial investigation of Goffaux [7], this work has converged to the most relevant formulation of the salvage value for the model EnergyScope. This aims at considering the residual value of assets that would still be

in place after the end of the optimisation. It avoids penalising capital-intensive and long-lasting asset. In this formulation, the capacities that have been anticipatively decommissioned are removed from the total installed capacities. Therefore, this penalises decisions that would lead to investments that are later decommissioned before having reached the end of their lifetime.

Other authors' main contribution statement

Novelty does not stand in the reinvention of the wheel. This thesis, instead, finds its fundamentals in great tools previously developed by other authors. As developers of the building blocks of the main contributions of this thesis, three main authors are to be mentioned for having brought a significant part of the methodological work. Based on Stefano Moret's monthly whole-energy system model (i.e. EnergyScope) [8], Gauthier Limpens has developed the hourly version of the snapshot model (i.e. EnergyScope TD) [9], as well as the perfect foresight pathway model [10], to which I personally contributed too. Diederik Coppitters has developed the RHEIA framework allowing to quantify the impact of uncertainties and carry out robust optimisation of energy systems [11]. The current work used this framework for the first of these functionalities. Finally, Stefano Moret extensively assessed the uncertainty characterisation on the Swiss energy system [4]. This thesis follows the same methodology, updating the uncertainty ranges for the pathway model.

1.1 Whole-energy system transition model optimisation: EnergyScope Pathway

This work optimises the entire transition pathway from a known system in 2020 up to 2050 thanks to EnergyScope Pathway [10]. According to pathway models review (see Appendix ??), EnergyScope Pathway can be categorised as an investment and operation optimisation model that assesses the whole-energy system, has a hourly time-resolution and is an open-source documented model. Moreover, it maintains a low computational cost (i.e. around 15 minutes for a 30-year pathway with a hourly discretisation). From the perfect to the myopic foresight of the transition optimisation, this section presents only the main constraints of the former approach to further dig into more details about the latter. The reader is invited to refer to Appendix ?? for more details about the formulation of the model and its extension from, EnergyScope TD, the a snapshot model, optimising a target future year with a greenfield approach

[12]. More extensive information about the formulation choices, for instance, can be found in [10] and the documentation [13].

1.1.1 Perfect foresight: One global optimisation of the transition

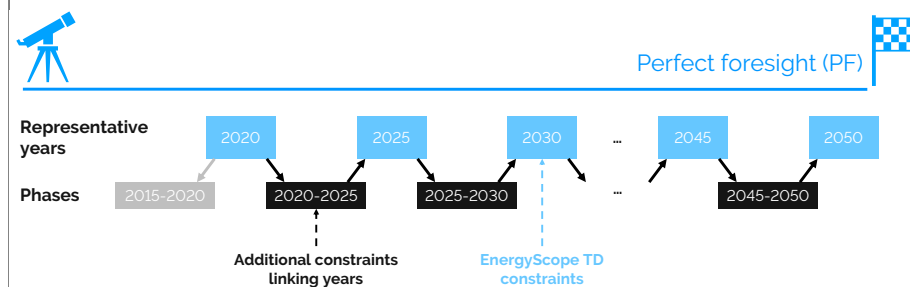


Figure 1.1. Illustration of the pathway methodology based on an existing energy system model. The methodology spans from 2020 to 2050, with one representative year every five years. The model EnergyScope Typical Days (EnergyScope TD) is applied in 7 representative years (light blue boxes). The formulation includes additional constraints (black boxes) that link the years together. The pathway's initialisation assumes that all capacities installed in 2020 were built during the pseudo-phase of 2015–2020 (grey box). The overall problem is defined as the pathway model.

The whole-energy system model developed in this work originates from the perfect foresight (PF) formulation (Figure 1.1) of EnergyScope—the entire transition is computed in one optimisation, assuming a complete but uncertain knowledge of the different parameters until 2050 [10]. Each representative year is represented via the variables and constraints of the snapshot model, EnergyScope TD [9]. Then, to draw a consistent pathway between these years, additional constraints aim at linking them, e.g. limiting the modal shifts within some energy sectors.

The objective function of the pathway model, i.e. the total transition cost $C_{\text{tot,trans}}$, is computed as the sum of the total capital expenditure (CAPEX), $C_{\text{tot,capex}}$, and the operational expenditure (OPEX), $C_{\text{tot,opex}}$ (see Eq. 1.1).

$$\min C_{\text{tot,trans}} = C_{\text{tot,capex}} + C_{\text{tot,opex}} \quad (1.1)$$

The total CAPEX is the difference between the total investments done during the transition, $C_{\text{inv,phase}}$, and the residual value of the assets that would still be in place after the end of the transition, $C_{\text{inv,return}}$ (see Eq. 1.2).

$$C_{\text{tot,capex}} = \sum_{p \in \text{PHASE} \cup \{2015_2020\}} C_{\text{inv,phase}}(p) - \sum_{j \in \text{TECH}} C_{\text{inv,return}}(j), \quad (1.2)$$

where $C_{\text{inv,phase}}$ is given as the sum over all the newly installed technologies at the phase p , $F_{\text{new}}(p)$, multiplied by the average investment costs, c_{inv} , of the year starting and ending the corresponding phase, y_{start} and y_{stop} respectively (see Eq. 1.3).

$$C_{\text{inv,phase}}(p) = \sum_{j \in \text{TECH}} F_{\text{new}}(p, j) \cdot \tau_{\text{phase}}(p) \cdot c_{\text{inv}}(p, j) \quad \forall p \in \text{PHASE}, \quad (1.3)$$

where τ_{phase} is the annualised phase factor and $c_{\text{inv}}(p, j)$ is the arithmetic average of the investment cost of the technology j at the beginning and the end of the phase, $c_{\text{inv}}(y_{\text{start}}, j)$ and $c_{\text{inv}}(y_{\text{stop}}, j)$. Similarly, the salvage value is computed in the proportion of the remaining years of life versus the initial lifetime of an installed capacity of a technology from which the anticipatively decommissioned part, F_{decom} , is removed (see Eq. 1.4)

$$C_{\text{inv,return}}(j) = \sum_{p \in \text{PHASE} \cup \{2015_2020\}} \tau_{\text{phase}}(p) \cdot c_{\text{inv}}(p, j) \cdot \frac{\text{remaining_years}(j, p)}{\text{lifetime}(y_{\text{start}}, j)} \left(F_{\text{new}}(p, j) - \sum_{p2 \in \text{PHASE}} F_{\text{decom}}(p2, p, j) \right) \quad \forall j \in \text{TECH} \quad (1.4)$$

About the total OPEX of the transition, $C_{\text{tot,opex}}$, on top of the initial costs in 2020, we assume that the OPEX of a phase is equal to the average operational costs, C_{opex} , of y_{start} and y_{stop} , multiplied by the duration of a phase t_{phase} equal to 5 years in our case (see Eq. 1.5).

$$C_{\text{tot,opex}} = C_{\text{opex}}(2020) + t_{\text{phase}} \cdot \tau_{\text{phase}}(p) \cdot \sum_{p \in \text{PHASE}} C_{\text{opex}}(p), \quad (1.5)$$

where $C_{\text{opex}}(p)$ is the arithmetic average of the operational cost at the beginning and the end of the phase p , $C_{\text{opex}}(y_{\text{start}})$ and $C_{\text{opex}}(y_{\text{stop}})$. The operational cost of a year, y , $C_{\text{opex}}(y)$, is the sum of the costs related to maintenance and operation of technologies, C_{maint} , and the consumption of resources, C_{op} (see Eq. 1.6).

$$C_{\text{opex}}(y) = \sum_{j \in \text{TECH}} C_{\text{maint}}(y, j) + \sum_{i \in \text{RES}} C_{\text{op}}(y, i) \quad \forall y \in \text{YEARS}, \quad (1.6)$$

where the costs related to each representative year are:

$$C_{\text{maint}}(y, j) = c_{\text{maint}}(y, j) \mathbf{F}(y, j) \quad \forall y \in \text{YEARS}, \forall j \in \text{TECH} \quad (1.7)$$

$$C_{\text{op}}(y, i) = \sum_{t \in T} c_{\text{op}}(y, i) \mathbf{F}_t(y, i, t) t_{\text{op}}(t) \quad \forall y \in \text{YEARS}, \forall i \in \text{RES}, \quad (1.8)$$

where the variable \mathbf{F} represents the size of the installed capacities (for all technologies j) and the variable \mathbf{F}_t is the hourly consumption of the resources; the parameter c_{maint} is the OPEX of the technologies, and the parameter c_{op} is the cost of purchasing resources. For the sake of simplicity, as done by Limpens et al. [10], the sum over the 8760 hours of the year is written as the sum over $t \in T$.

The CO₂-budget for the transition, $\mathbf{GWP}_{\text{tot,trans}}$ is equal to the arithmetic average of the representative years at the beginning and the end of each phase (see Eq. 1.9). Similarly to initial operational costs to account for the system in place in 2020 (see Eq. 1.5), $\mathbf{GWP}_{\text{tot}}(2020)$ accounts for the entire operational emissions in 2020, as the initial cumulative emissions of the transition. Then, as detailed in Section ??, these cumulative emissions is constrained by a budget (see Eq. 1.10).

$$\mathbf{GWP}_{\text{tot,trans}} = \mathbf{GWP}_{\text{tot}}(2020) + t_{\text{phase}} \sum_{p \in \text{PHASE}} \mathbf{GWP}_{\text{tot}}(p) \quad (1.9)$$

$$\mathbf{GWP}_{\text{tot,trans}} \leq gwp_{lim,trans}, \quad (1.10)$$

where $\mathbf{GWP}_{\text{tot}}(p)$ is the arithmetic average of the yearly emissions at the beginning and the end of the phase p , $\mathbf{GWP}_{\text{tot}}(y_{\text{start}})$ and $\mathbf{GWP}_{\text{tot}}(y_{\text{stop}})$. The computation of these yearly emissions are based on the global warming potential (GWP) of the resources:

$$\mathbf{GWP}_{\text{tot}}(y) = \sum_{i \in \text{RES}} \mathbf{GWP}_{\text{op}}(y, i) \quad \forall y \in \text{YEARS} \quad (1.11)$$

$$\mathbf{GWP}_{\text{op}}(y, i) = \sum_{t \in T} gwp_{op}(y, i) \mathbf{F}_t(y, i, t) t_{\text{op}}(t) \quad \forall y \in \text{YEARS}, \forall i \in \text{RES}, \quad (1.12)$$

where gwp_{op} is the specific emissions (i.e. in kt_{CO₂,eq}/GWh) of each resource. Based on an approach developed by the Intergovernmental Panel on Climate Change (IPCC) [14], this work considers the indicator “GWP100a - IPCC2013” to compute the emissions related to the use of resources. This includes the emissions due to the extraction, the transportation and the combustion of the energy carrier. EnergyScope proposes to account for the embodied emissions of the technologies based on a life cycle assessment (LCA). These stand for extraction of materials, refining, construction and end of life [15]. However, this work is still in progress and the database is not yet complete. Consequently, it is not included in this work and not accounted for.

Besides this constraint on the emissions, the main constraint to link years with each other is the one dictating the installed capacities at the end of each year:

$$F(y_{stop}, j) = F(y_{start}, j) + F_{new}(p, j) - F_{old}(p, j) - \sum_{p2 \in PHASE \cup \{2015_2020\}} F_{decom}(p, p2, j)$$

$$\forall p \in PHASE, y_{stop} \in Y_STOP(p), y_{start} \in Y_START(p), j \in TECH \quad (1.13)$$

where the variables F_{old} and F_{decom} are the capacities respectively having reached the end of their lifetime and prematurely decommissioned. Moreover, to account for the society inertia and to prevent unrealistically fast modal share change, constraints limit this change for the sectors of the low-temperature, the passenger mobility and freight mobility demands. The interested reader will find more information about the formulation choices related to it in the work of Limpens et al. [10].

1.1.2 Myopic: Sequential optimisation of the transition with limited foresight

One of the main methodological contributions of this work regarding the development of the whole-energy system model consists in giving it the possibility to optimise the transition pathway in a myopic approach. After introducing the general concept of it, this section details more the additions brought to the model in terms of implementation.

General concept of the myopic optimisation

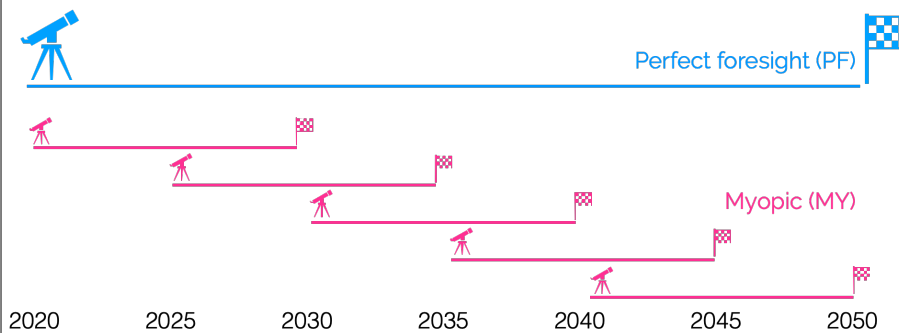


Figure 1.2. The myopic approach (in pink) uses several instances of the pathway model (illustrated in Figure ??). In this example, the pathway instance has a time horizon of 10 years ($N_{year,opti} = 10$) with a 5 year-overlap ($N_{year,overlap} = 5$). As a comparison the Perfect foresight (in blue) has a time horizon of 30 years.

Compared to the perfect foresight, the myopic approach (Figure 1.2) has two main advantages: shorter computational time and more realistic representation of the short-sightedness of decision-makers. For this reason, several studies are based on this approach [2, 16–18]. Babrowski et al. [2] analysed the benefit of the myopic approach to reduce the computational time. Poncelet et al. [16] uses this approach to analyse the expansion planning of the power sector beyond 2050 to assess the realism of the decision making process brought up by the myopic implementation. Nerini et al. [17] analysed the impact of the horizon windows and overlapping time. Overall these studies decided to choose the myopic approach to analyse the speed of change compared to a perfect foresight approach. Moreover, the myopic approach allows a sequential optimisation process that opens the doors to decision-making/policy-learning methodologies, like assessing shock events. This approach is used by Heuberger et al. [18] who assessed the speed of integration of technologies due to these events. In their analysis of the overcapacity in European power systems, Moret et al. [19] emphasised that such a “possibility of *recourse*” is very appropriate to address uncertainty gradually unfolding over time. Consequently, the development of the myopic approach with an overlap between two successive time windows has been implemented. This sequential optimisation framework also represents the foundations of the further implementation of the agent-based reinforcement learning framework (see Section 1.3).

As illustrated in Figure 1.3, after optimising, in design and operation, one time window (e.g. from 2020 to 2030), the intermediate system design (i.e. the installed capacities) is set as initial conditions for the start of the next time window (e.g. from 2025 to 2035) as well as the historical investment decisions (i.e. \mathbf{F}_{new} , \mathbf{F}_{old} and $\mathbf{F}_{\text{decom}}$). Consequently, the solution obtained at the end of the first time window (e.g. 2030) as well as potential investment decisions between the start of the second time window and this end-year are discarded. In other words, they are not taken into account for the optimisation of the second time window since the new final year is further into the future. This process goes on until the stated end of the transition (i.e. 2050, in this case).

Additional sets, parameters and variables

The major add-on from the original EnergyScope Pathway model [1] to the myopic version developed in this thesis, is the possibility to carry out the optimisation on a limited time window, of which the duration is defined by $N_{\text{year,opti}}$. Moreover, there is also the possibility of having an overlap between two consecutive time windows. The timespan of this overlap is defined by the parameter $N_{\text{year,overlap}}$. The philosophy followed behind the development of the myopic approach was to add another layer on top of the perfect foresight model in order to make it more modular. For this reason,

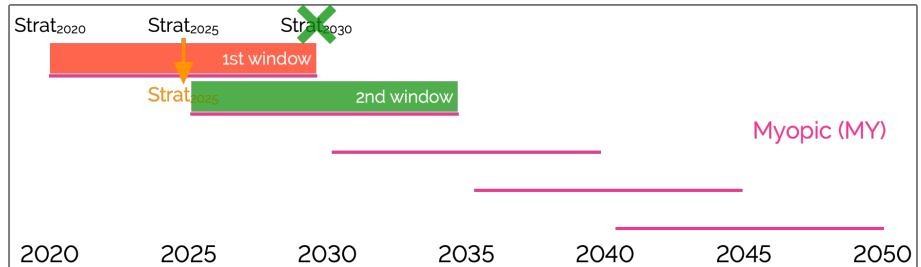


Figure 1.3. Sequential optimisation of the transition pathway in the myopic approach: (i) first time-window optimisation, (ii) set-up of the initial conditions of the second time-window, (iii) second time-window optimisation discarding intermediate results

the already existing constraints are marginally adapted. This way, the newly developed model can easily be used to perform a perfect foresight optimisation by setting the time window to $N_{\text{year, opti}} = 30$ years (i.e. between 2020 and 2050) and the overlap between the time windows to $N_{\text{year, overlap}} = 0$. Consequently, as it is fundamental to define, on the one hand, the actual time window on which the system is optimised, and on the other hand, the history, i.e. what has already been optimised earlier in the transition, four new sets are implemented: YEARS_{WND}, YEARS_{UP TO}, PHASE_{WND} and PHASE_{UP TO} (see Table 1.1).

Table 1.1. New SETs for myopic pathway formulation.

Set	Index	Description
YEARS _{WND}	$y \in Y$	Representative years of the time window to optimize
YEARS _{UP TO}	$y \in Y$	Representative years including the years already optimised, i.e. the history
PHASE _{WND}	$p \in P$	Phases of the time window to optimize
PHASE _{UP TO}	$p \in P$	Phases including the phases already optimised, i.e. the history

YEARS_{WND} and PHASE_{WND} substitute YEARS and PHASE in the constraints defined in the pathway model in Section 1.1.1. These two sets aim at setting the optimisation to a more limited time window. Progressing through the transition, YEARS_{UP TO} and PHASE_{UP TO} allow keeping track of the history of the investments (e.g. technologies installation, decommissioning or retirement), the consumption of resources, the cumulative amount of emissions, etc.

On top of these four specific sets, some artefacts were also necessary to avoid computational rounding errors. For instance, the first year of a time window is the result of the optimisation of the previous one. Therefore, optimising again this first year could lead to rounding errors preventing from the optimization to converge. For this reason, the set YEAR_{ONE} accounts for the first representative year of the time window to optimize that is excluded from $\text{YEARS}_{\text{WND}}$ to avoid these errors. This remark stays valid for any time window except the first one of the transition where the year 2020 is optimized even though its technological strategy is set according to the actual system presented in Appendix ???. Finally, as the end of time windows changes for each of them, the parameter *remaining_years* has to be updated accordingly to keep a meaningful definition of $C_{\text{inv},\text{return}}$ in Eq. 1.4.

Myopic pathway implementation

Starting this work in 2017, AMPL Optimization Inc. has developed a Python application programming interface (API) called `amplpy` [20]. In a nutshell, this API allows the pre/post-processing of an `ampl` optimisation problem by accessing its features (e.g. constraints, parameters, variables, objective function) from within Python. Using this API, this updated version of the model interacts with the AMPL problem representing the optimization of the whole-energy system transition pathway as represented in Figure 1.4.

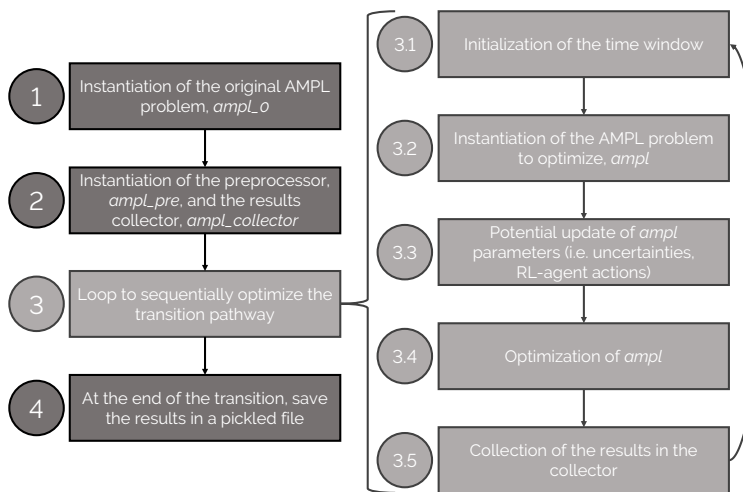


Figure 1.4. Schematic of the iterative optimization of the whole-energy system transition pathway.

Impact of myopic formulation on the system

In line with the work of Babrowski et al. [2], the computational time is reduced drastically (i.e. by 55%). On top of this, we observed that the resulting design, i.e. the technological mix, remains similar. Given the continuous change of the input parameters over the considered time frame, the perfect foresight and myopic approaches results are very similar, like in [21]: less than 1% cost difference over the transition, similar system designs by 2050 and slight shifts in time in terms of adoption of technologies.

The main difference lies in the myopic transition itself and especially in the earlier deployment of PVs and offshore wind turbines. These induce the reinforcement of the grid that is a capital-intensive and long-lifetime asset. This is mostly due to impact of the salvage value, Eq. 1.4, in the objective function. Since this is now the transition cost over a more limited time window (i.e. 10 years rather than 30 years), a bigger salvage value, deduced from the total investments, leads to a temporary better optimum at early stages of the transition. A more detailed comparison between the myopic and perfect foresight approaches is available in Appendix ??.

1.2 Uncertainty quantification

In their systematic review, Yue et al. [22] highlighted that a wide majority of studies addressing the optimisation of energy systems (i.e. 75% out of the 134 reviewed studies) were not investigating the impact of uncertainties. However, disregarding these impacts can have drastic consequences on the system design. For instance, historical low fossil gas (NG) prices have led to overcapacity of combined cycle gas turbine (CCGT) in Europe [19]. This is why accounting for uncertainty in energy system optimisation models (ESOMs) is crucial [23], especially when it comes to optimise several decades in an inherently uncertain future [24].

This section aims at briefly presenting the methods followed to first characterise these uncertainties, then to quantify their impact on different outputs of interest of the model (e.g. amount of molecules imported from abroad, the installed capacity of small modular reactor (SMR) or the total transition cost) and finally, the screening and selection of the parameters to analyse.

1.2.1 Uncertainty characterisation

Characterising precisely the uncertainty—ideally with their respective probability density functions (PDFs)—of the thousands of parameters in the model is daunting if not impossible because of lack of data [25]. Therefore, we used a workaround developed

by Moret et al. [4] that defines relative ranges of variation for different groups of parameters. These ranges have been adapted for the Belgian energy system and the pathway formulation. Moreover, some ranges have been added to account for new parameters coming from the pathway formulation described in Section 1.1 like the society inertia. Like other works [26, 27] and given the scarcity of information, the uncertain parameters are assumed to be independent and uniformly distributed between their respective lower and upper bounds. Alternatives like PERT or Gaussian distributions could also have been considered [11].

Following the methodology defined by Moret et al. [4], uncertainties of types I (investment-type) and II (operation-type, constant uncertainty over time) keep the same range width for the whole transition. In other words, unlike type III parameters, this width is not expanding (nor narrowing) for the different representative years of the transition. However, parameters with an uncertainty increasing over time, type III, (i.e. end-use demands, in this case) will have a wider and wider range over the transition (see Figure 1.5). In this work, a +50% linear increase has been set between the width of the range of such parameters in 2025 and the same ranges in 2050. This choice leads to an industrial end-use demand (EUD) that could be, in 2050, -30.8% compared to its nominal value. This potential drop compared to the reference is in line with the work of Climact and VITO [28]. In their work, the total energy demand in the industry sector in 2050 could be between -19% to -50% of the reference value, depending on the scenario. In Figure 1.5, this means that for type III uncertainties only, R_{2050}^+ is 50% bigger than R_{2025}^+ and R_{2050}^- is 50% smaller than R_{2025}^- . For uncertainties of types I and II, the relative variation versus the nominal value remain the same over the transition. Inspired by Guevara et al. [3], the values of the uncertain parameters are set at a fixed relative position from the nominal values for each sampled transition—the values do not zigzag from 2025 to 2050 within the bounds (Figure 1.5).

Finally, the model accounts for thousands of parameters. The computational burden to consider all of them separately would be completely overwhelming ($\sim 10^7$ model runs¹). Similarly to other works [4, 5], the model parameters that would follow the same uncertainty have been grouped to one single uncertain parameter. On top of mitigating the computational burden, this aims at grouping parameters that are closely linked with each other. For instance, the uncertainty on the cost of purchasing renewable electrofuels, $c_{\text{op,electrofuels}}$, identically affects the cost of e-hydrogen, e-methane, e-ammonia and e-methanol. Indeed, besides their respective specificities, each of these

¹ As detailed in Section 1.2.2, the number of runs required for the GSA is proportional to the factorial of the number of uncertain parameters. As second order Polynomial Chaos Expansion (PCE) is the minimum to ensure accuracy of the surrogate model, considering thousands of independent uncertain parameters would lead to millions of runs, if no more.

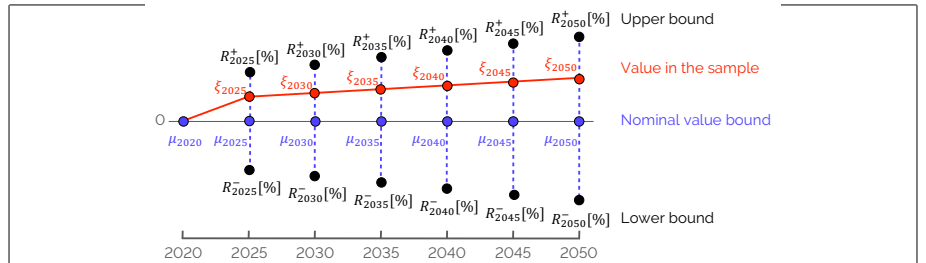


Figure 1.5. Expansion of the width of uncertainty range for type III parameters. $\mu_{2020}, \mu_{2025}, \dots, \mu_{2050}$ are the nominal values equal to 0 as the uncertain parameters represent a relative increase/decrease of actual parameters of the model. R^+ and R^- are respectively the upper and lower bounds of the range and $\xi_{2025}, \xi_{2030}, \dots, \xi_{2050}$ are the values taken by one parameter for a specific sample of the global sensitivity analysis (GSA) for each of the representative years of the transition, always starting from the nominal value in 2020, μ_{2020} . The graph has been adapted from [3].

fuels will be similarly affected by the variation of cost of electricity or the electrolyser, that drive the majority of their cost of purchasing [29]. Similarly, the uncertainties impacting the industrial demand, *industry_EUD*, alters equally the industrial high- and low-temperature and electricity demands as well as the non-energy demand.

1.2.2 Polynomial Chaos Expansion

To avoid the computational burden of well-known method like Monte-Carlo analysis [22], we used PCE to carry out a GSA. PCE is an approach for surrogate-assisted uncertainty quantification (UQ) that propagates uncertainties in input parameters through the system model. This allowed us to assess statistical moments on the quantity of interest and determine Sobol' indices [30]. To construct a PCE of the EnergyScope Pathway model, we employed the open-source Python framework RHEIA [31, 32]. Where the first part of this section is dedicated to the mathematical definition of this approach, the second details its choice and summarises the comparison made with another approach (i.e. Morris method) in a previous work [5].

Definition

The PCE model (\hat{M}) is a representation of the relationship between the input parameters and the output variable of interest (i.e. the value of the objective function, see Eq. 1.1) in the EnergyScope Pathway model (M). This representation is constructed as a

truncated series of multivariate orthonormal polynomials Ψ , weighted by coefficients u :

$$\hat{M}(\xi) = \sum_{\alpha \in \mathcal{A}^{d,p}} u_\alpha \Psi_\alpha(\xi) \approx M(\xi), \quad (1.14)$$

where the vector $\xi = (\xi_1, \xi_2, \dots, \xi_d)$ comprises the independent random input parameters (??), d corresponds to the number of input distributions and α is a multi-index, i.e. a vector of non-negative indices of length d , where each index corresponds to the degree of each univariate polynomial that forms the basis of the multivariate polynomial Ψ_α . The coefficients $(u_0, u_1, \dots, u_{P+1})$ are quantified using a regression method applied to orthonormal polynomials [33]. As uniform distributions are considered, the Legendre polynomials are adopted, as they are the associated family of polynomials that are orthogonal with respect to standard uniform distributions [33].

A truncation scheme is implemented to restrict the number of multivariate polynomials in the series. This is done based on two factors: a specified limiting polynomial order (p) and the number of uncertain parameters (d) involved. The multivariate polynomial order $|\alpha|$ is the summation of the orders for each univariate polynomial in the multivariate polynomials space. Thus, only the multi-indices corresponding to an order that is less than or equal to the specified limiting order are retained and stored in the truncated series denoted as $\mathcal{A}^{d,p}$:

$$\mathcal{A}^{d,p} = \{\alpha \in \mathbb{N}^d : |\alpha| \leq p\}. \quad (1.15)$$

The number of multi-indices satisfying this condition is as the cardinality of \mathcal{A} , i.e. the number of its elements:

$$\text{card}(\mathcal{A}^{d,p}) = \binom{p+d}{p} = \frac{(d+p)!}{d!p!} = P + 1. \quad (1.16)$$

To ensure a well-posed least-square minimisation, it is recommended to have a number of training samples at least twice the number of coefficients [33]. Therefore, $2(P + 1)$ samples are evaluated in the system model, and the model response for each quantity of interest is recorded. To generate the training samples, the quasi-random Sobol' sampling technique is employed [34]. As a low-discrepancy sequence, this technique exhibits the main advantage to investigate efficiently and (almost) uniformly the hypercube of uncertainties, unlike uniformly distributed random numbers.

The process of defining the polynomial degree includes incrementally increasing it until a desired level of accuracy is achieved [31]. Starting with $p = 1$, a PCE is constructed and the leave-one-out (LOO) error is evaluated. If the LOO error is below a specified threshold ($\sim 1\%$), the corresponding polynomial order is considered

sufficient for generating an accurate PCE. However, if the error exceeds the threshold, the order is increased, and additional samples are generated following the rule of Eq. (1.16).

For the specific study of this work, a polynomial order of 2 is necessary (with 1260 training samples as per Eq. (1.16)) to achieve a LOO error below 1 % for the total transition cost.

Lastly, the statistical moments can be analytically derived from the PCE coefficients, eliminating the need for further model evaluations. The mean μ and standard deviation σ are obtained as follows:

$$\mu = u_0, \quad (1.17)$$

$$\sigma^2 = \sum_{i \neq 0} u_i^2. \quad (1.18)$$

Furthermore, the Sobol' indices can also be determined analytically. The total-order Sobol' indices (S_i^T) assess the overall influence of a stochastic input parameter on the performance indicator, encompassing all possible interactions:

$$S_i^T = \sum_{\alpha \in A_i^T} u_\alpha^2 / \sum_{i=1}^P u_i^2 \quad A_i^T = \{\alpha \in A | \alpha_i > 0\}. \quad (1.19)$$

Here, A denotes the collection of all PCE coefficients, and α_i corresponds to the coefficient associated with the uncertain parameter i .

Comparison with a proven method

Besides being an in-house used method, an early step of this thesis consisted in assessing PCE with similar approach used in the literature [5].

After characterising the uncertainty ranges, Moret et al. [4] quantified the impact of these uncertainties on the snapshot model of EnergyScope, i.e. ranking them, using the Morris method [35]. This method, as a statistical analysis, relies on individually randomized one-factor-at-a-time designs. Given the d model parameters $\vec{\xi} = (\xi_1, \xi_2, \dots, \xi_d)$, the first step of the method consists in generating independent random samples of $\vec{\xi}$ in a standardised and discretised p -level *region of experimentation*, ω . In this *region of experimentation*, each ξ_i , varying in the interval $[\xi_{i,min}, \xi_{i,max}]$, can take a random discrete value as follows :

$$\xi_i = \xi_{i,min} + j \cdot \frac{1}{p-1} (\xi_{i,max} - \xi_{i,min}) \quad \text{with } j \in \{0, 1, \dots, p-1\} \quad (1.20)$$

Then, given these random one-factor-at-a-time samples, Morris method defines, for a given set of $\vec{\xi}$, the elementary effect of the i th parameter (EE_i) as :

$$EE_i = \frac{M(\xi_1, \xi_2, \dots, \xi_i + \Delta, \dots, \xi_d) - M(\vec{\xi})}{\Delta}, \quad (1.21)$$

where M is the objective function, $\vec{\xi} \in \omega$, except $\xi_i \leq 1 - \Delta$ and Δ is a set multiple of $1/(p-1)(\xi_{i,max} - \xi_{i,min})$. As in other studies [4, 36, 37], we consider p as even and $\Delta = p/[2(p-1)](\xi_{i,max} - \xi_{i,min})$.

Finally, in order to evaluate the importance of the i th parameter over an output, Morris method relies on F_i , the distribution of r elementary effects. Computing the mean, $\mu_i = \mu(F_i)$, and the standard deviation, $\sigma_i = \sigma(F_i)$, of the F_i distribution, allows ranking the parameters based on their influence on the concerned output. Usually, in Morris method, p and r respectively get values as follows : $p \in \{4, 6, 8\}$ and $r \in [15; 100]$ depending on, d , the number of uncertain parameters. The higher this number is, the higher shall be, simultaneously, p and r . In the following comparative analysis, we set p and r to their maximum values, respectively 8 and 100 in order to get the most reliable parameters ranking.

Beyond the original Morris method, we used the standardized elementary effects, SEE_i , formulation [36], given by

$$SEE_i = EE_i \cdot \frac{\sigma(\xi_i)}{\sigma(M)}. \quad (1.22)$$

Among other things, the SEE allows comparing the influence of different inputs on the same output or compare the influence of a same parameter on different outputs, even if these parameters or outputs are significantly different in terms of variation range or average amplitude. Moreover, this standardized analysis does not require any additional model evaluations.

Therefore, in the following results, we rather use

$$\mu_i^* = \mu(|SF_i|) \quad (1.23)$$

to rank parameters among each other. In (1.23), SF_i is the distribution formed by the r standardized elementary effects, as done in Moret [37].

In [5], we have assessed the PCE approach, comparing the Top-14 most impacting parameters obtained from this approach with the one provided by the improved Morris method based on μ_i^* . Even if the output of each method does not have the same physical

meaning, both methods can rank the parameters by their impact on the total annual cost of the energy system. Both rankings were very similar which validates the use of PCE in the rest of this work.

1.2.3 Preliminary screening and selection

After the initial phase of grouping (Section 1.2.1), a preliminary screening was necessary to identify the key parameters to account for in this GSA. Rixhon et al. [6] performed a similar sensitivity analysis on the 2050 Belgian whole-energy system under different CO₂-limits using the snapshot model, i.e. EnergyScope TD [9]. Screening the results of this work, we have discarded some parameters with negligible impact² (e.g. CAPEX of electrolyzers or variation of the freight demand), selected a subset of parameters and added others that were intrinsic to the pathway formulation, e.g. modal share changes, or related to the integration of SMR, $f_{\max, \text{SMR}}$. The exhaustive list of these 34 parameters is presented in Appendix ??.

1.3 Agent-based reinforcement learning for energy transition support

The transition towards carbon-neutrality of a whole-energy system (i.e. including all streams of energy carriers and demands) is uncertain. Therefore, instead of establishing single-shot definitive plans towards 2050 (and beyond), policy makers rather go through multiple rolling-horizon short-term decisions. Yet, these decisions can have long-term impacts, 20 to 50 years. This long-term future is intrinsically uncertain and could be the place for potential sudden unexpected events. Meeting the environmental objectives while minimizing the cost of the system, accounting for this decision-making process, the uncertainties, and potential shocks/crisis, require therefore a framework to assess the relevance and the timing of the decisions throughout the transition. To navigate through the transition and investigate the efficiency of different policies, this work implements the reinforcement learning approach. This section aims at presenting the general concepts of this approach. Then, its application to the myopic optimisation of a whole-energy system is introduced as well as the policy optimisation algorithm.

²Per Turati et al. [38], parameters are considered as “negligible” if their Sobol’ index is below the threshold = $1/d$, d being the total number of uncertain parameters

1.3.1 Reinforcement learning fundamentals and application to energy systems

RL is a subfield of machine learning focused on training an agent to make sequential decisions by interacting with an environment to achieve specific goals (see Figure 1.6). Unlike supervised learning, where data is labelled, and unsupervised learning, where patterns are inferred from unlabelled data, reinforcement learning deals with learning from interaction, typically through trial and error. This way, RL is considered as active learning [39]. Starting from an initial state, the agent takes an action that impacts its environment. The latter feeds back the agent with a reward and the new state (see Figure 1.6). This goes on until reaching the end of the episode. When the episode is done, the agent starts again from an initial state, takes an action and so on.

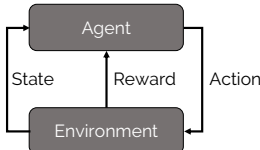


Figure 1.6. General concept of reinforcement learning (RL) as the interactions between the agent and its environment. The agent takes some action that has an impact on the environment which feeds back the agent with a reward and the new state. The objective of the agent is to optimize its policy, i.e. mapping between the state it is at and the action to take, by maximizing its cumulative reward.

The agent learns to optimize its policy by maximizing a notion of cumulative reward over time. This policy refers to the strategy or mapping from states to actions that the agent employs to make decisions. Essentially, it defines the behavior of the agent in the environment. The ultimate goal of the agent is often to find an optimal policy, which maximizes the expected cumulative reward over time. All these concepts and interactions between the agent and its environment are formalized as a Markov decision process (MDP) [40], represented by the tuple $\langle s, a, T, r, \pi, \gamma \rangle$. The Markov property of such a decision process states that a decision is made only based on this tuple and not on the history/path that has led to it. In this tuple, $s \in S$ is the state defined in a certain state space, S , that represents the observable parts of the environment that the agent uses to make decisions; $a \in A$ is the action among the action space, A ; T is the probability of transitioning from one state s to another state s' given a specific action, a : $T(s, a, s') : \Pr(s'|s, a)$; r is the reward received by the agent when taking the action a from state s , $R(s, a)$; π is the policy telling the action to take depending on the current state and; γ is the discount factor that controls the importance of future re-

wards versus immediate rewards. During the learning/optimization process, the agent acts according to the exploitation-exploration trade-off. In the exploitation, the action a is directly given by the mapping provided by the current policy π , depending on the state s . In the exploration, the action is randomly picked within the action space. For further information, the interested reader is invited to refer to work of Sutton and Barto [40] or the course given by David Silver [41] available online.

Due to the increasing complexity of the systems and the integration of uncertainties, the last decades have seen the emergence of publications where RL is applied to energy systems [39, 42]. In their respective reviews, Cao et al. [39] and Perera and Kamalaruban [42] highlighted groups of problems addressed with RL in the research field of energy systems: building energy management system (BEMS), optimization of dispatch and operational control closely linked with the energy market and the optimal power flow problem in the grid, micro-grid management, electro-mobility or even demand-side management or optimal control of energy system devices like maximum power point tracking (MPPT) of wind turbines and photovoltaic (PV) panels. The major novelty of this thesis is the application of RL to a new kind of energy system problem: the optimization of the transition pathway of a whole-energy system. In this sense, the objective is to optimize and provide a policy to support this transition subject to uncertainties.

1.3.2 Problem formulation and algorithm

At the initial state, i.e. the energy system in 2020, the agent gets an initial observation, o_0 . An observation represents a set of the characteristics of the environment accessible to the agent for it to take the next action. The state, though, is the exhaustive list of these characteristics. Even though an observation is a subset of the state, this work uses these two words interchangeably. Then, it takes an action, a_0 , impacting its environment, i.e. the energy system limited transition over the first decision window (2020-2030). Through this interaction with its environment, the agent is given a reward, $r_1 = r(a_0|o_0)$, and ends up in a new state, i.e. the energy system in 2025, characterised by a new observation, o_1 , and so on (see Figure 1.7).

A learning episode is a succession of such learning steps. In the context of the transition pathway between 2020 and 2050, an episode can come to an end for different reasons. First, if the actions taken by the agent make the optimisation infeasible, the episode is prematurely stopped before reaching 2050. Similarly, cumulative emissions of the system over the predefined CO₂-budget (see Section ??) lead to an anticipated end of the episode. Finally, the “natural” end is the prescribed end of the transition, i.e.

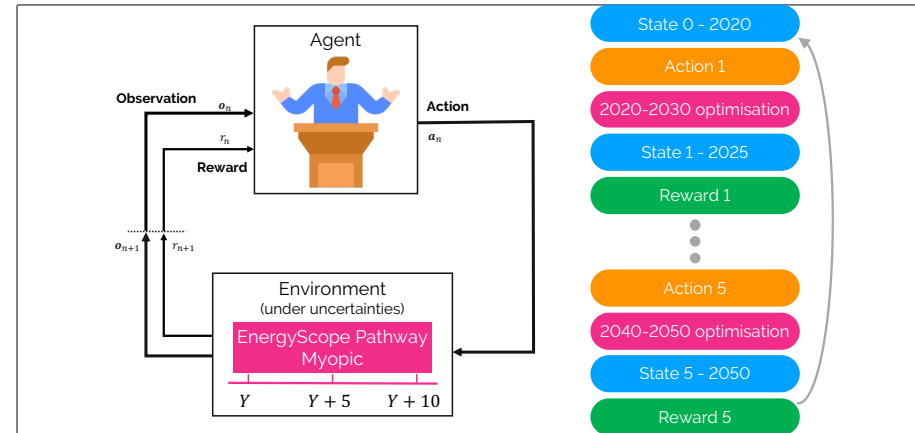


Figure 1.7. Reinforcement learning (RL) framework made of the agent interacting with its environment, i.e. the energy-system model on a limited decision window of 10 years.

2050. Consequently, the maximum value of steps for an episode is equal to $N_{ep,max} = 5$.

Before jumping to the choice of the learning algorithm, it is worth noting that we opted for the combination of RL with deep neural network (DNN), called deep reinforcement learning (DRL). Among others, one of the main drawbacks of traditional RL algorithms, i.e. without the use of neural network (NN), is that it suffers from the “curse of dimensionality” when facing problems with continuous action and state spaces (see Chapter ??). By approximating the state-action function with its parameters (i.e. weights and biases), DNN can address this difficulty.

Given the assumed absence of knowledge of the agent about the dynamics of the environment, i.e. its transition or reward functions, we needed a so-called “model-free” learning algorithm. In practice, in a model-free approach, the agent estimates the optimal policy directly from experience and without estimating the dynamics of the environment. However, model-free methods suffer from two major drawbacks: their sample inefficiency and their sensitivity with respect to their hyper-parameters (e.g. learning rates, exploration constants) [43]. The former leads to a too expensive computational burden while the second requires meticulous settings to get good results. To overcome these two challenges, we needed to choose between an “on-policy” or “off-policy” algorithm. In a nutshell, in on-policy learning, the agent learns the value function or policy based on the data it generates by following its current policy whereas, in off-policy, the agent can learn from data collected by any policy, not just the one it

is currently following, which provides greater flexibility and potential for reusing data. This makes off-policy algorithms more data efficient and ensuring better exploration by reusing past experiences or even following random exploration [43].

The goal of a RL approach is to optimise the mapping between inputs (i.e. the observations) and output (i.e. the actions), called the policy $\pi(a_n|o_n)$. To do so, an objective function, $J(\pi)$, is built on the cumulative rewards collected during each episode. Finally, a back-propagation process updates the weights and biases of the NN during the learning of the agent. Among the wide variety of RL algorithms applied in energy systems [42], this work opted for Soft Actor Critic (SAC) [43] to train and update the NN. Like other actor-critic-based algorithms, SAC works with two NN in parallel: the actor learning the control policy and the critic judging the actor (see Figure 1.8).

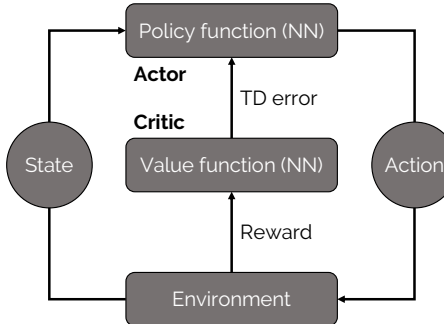


Figure 1.8. General concept of actor-critic-based algorithms. The two NN are trained against each other for the actor to improve the control policy and for the critic to provide a better judgement of the actor's action via the temporal-difference (TD) error. Graph adapted from [39].

SAC is a model-free and off-policy actor-critic deep RL algorithm based on the entropy-augmented³ objective function (see Eq. 1.24). Where entropy represents the amount of energy in a system not available to produce work in thermodynamics, this term, also called Shannon entropy in the RL context, stands for the randomness or stochasticity of the policy.

$$J(\pi) = \mathbb{E}_{\pi} \left[\sum_{n=0}^{N_{ep}} \gamma^n r_n(o_n, a_n) - \zeta \log(\pi(a_n|o_n)) \right], \quad (1.24)$$

³The word “augmented” here is in opposition to the conventional RL objective function that is only based on the cumulative reward, i.e. first term of Eq. 1.24.

where γ is the discount factor and ζ the temperature parameter. γ determines how much importance we want to give to future rewards within an episode. ζ balances the trade-off between exploitation of proven actions via the return maximisation, i.e. $\sum_{n=0}^{N_{ep}} \gamma^n r_n(o_n, a_n)$, and exploration through the entropy term, i.e. $\log(\pi(a_n|o_n))$. This way, SAC ensures sample efficiency while improving exploration [44] and robustness [45]. In their work, Haarnoja et al. [44] showed a lower sensitivity of SAC to hyper-parameters. These make SAC a state-of-the-art algorithm and one of the most efficient model-free deep RL method nowadays [44]. In this thesis, we used the open-source SAC package developed by STABLE-BASELINES3 [46] where the policy NN is a fully connected multilayer perceptron (MLP) built with TENSORFLOW [47]. For further information on RL and the SAC algorithm, the interested reader is invited to refer to the works of Sutton and Barto [40] and Haarnoja et al. [43], respectively.

1.4 Robustness assessment via PCA

When optimizing a transition pathway of a whole-energy system, including its uncertainties, capturing the most variable changes of design (i.e. installed capacities of each technology) can become overwhelming due to the curse of dimensionality. For the case study detailed in Chapter ??, this consists of i.e. 7 representative years of the transition (i.e. from 2020 to 2050), 113 possible technologies subject to uncertain parameters. To tackle this challenge, we have developed a methodology based on the Principal Component Analysis (PCA). The philosophy behind this approach is to identify key-combinations of design variables giving relevant dimensions to compare different systems, beyond their sole objective function, i.e. total transition cost, but without having to compare each design variable individually. This methodology provides two main outputs. First and foremost, using the model runs necessary to quantify the impact of the uncertain parameters on the total cost of the transition (see Section 1.2), it gives a metric on which to assess the robustness of energy transition policies resulting from different approaches. This metric gives more insight that, for instance, the variation of the total transition cost that encompasses too many aspects (i.e. design and operation strategies, variation along the transition) in one single value. Second, these “directions of variation” can highlight key modal shifts or highly varying design strategies over the transition. After introducing the general concept of PCA, this section aims at detailing the methodology proposed to give these “directions of variation” and to assess the robustness of policies.

1.4.1 Principal Component Analysis: General concept

Born in the early 20th century [48, 49], the Principal Component Analysis (PCA) finds its fundamentals from the singular value decomposition (SVD). SVD is a generalization, to an arbitrary (i.e. not especially square) matrix, of the spectral theorem stating that a normal matrix can be diagonalized by an orthonormal basis of eigenvectors. The core concept of principal component analysis (PCA) involves simplifying a dataset with numerous interconnected variables by reducing its dimensionality. The aim is to preserve as much variability within the data as feasible. This is accomplished by transforming the p -dimension data, \mathbf{x} , into a new set of variables called principal components (PCs), \mathbf{z} . These components are uncorrelated and arranged in such a way that the first ones retain the majority of the variability found in all of the original variables. On the other hand, the final principal components (PCs) pinpoint directions where there is minimal variation, indicating nearly constant linear relationships among the original variables [50].

The PCs are computed based on the covariance matrix of \mathbf{x} , Σ where the diagonal of this matrix gives the variance of the i^{th} variable and the other elements give the covariance between the i^{th} and the j^{th} variables where $i \neq j$. Out of this matrix, α_k is the eigenvector of Σ corresponding to its k^{th} highest eigenvalue λ_k . One crucial aspect of these eigenvectors is their normalization, i.e. $\alpha_k^T \alpha_k = 1$ [50]. This normalization has several objectives. Among them, this ensures orthogonality of the PCs ensuring that they represent independent directions in the original feature space. Then, normalizing the eigenvectors ensures that the magnitude of each eigenvector represents the importance or variance explained by its corresponding principal component. This makes it easier to interpret the relative importance of each principal component in explaining the variability of the data. Finally, this ensures a fair comparison between the original features. Without normalization, variables with larger scales would dominate the principal components, potentially skewing the results and leading to misinterpretation of the principal components. In other words, given this normalization, $\text{var}(z_k) = \lambda_k$, where $\text{var}(z_k)$ is the variance of z_k . Moreover, this means that α_{ki} , i.e. the component of α_k related to the i^{th} original variable, x_i , gives its weight in the k^{th} PC, i.e. z_k . This PC captures λ_k variance of the original data. In other words, a high absolute value of α_{ki} means that x_i has a significant impact in the direction given by the k^{th} PC [51].

Easier to represent in two dimensions, let us consider a vector \mathbf{x} composed of the variables x_1 and x_2 , $p = 2$, and 25 realisations of them (See Figure 1.9).

From these observations, the main objective of PCA is to find the linear combination, i.e. projection, of the original variables that maximize their spread, i.e. variance (see 1.10). Another way to understand this is to look at the other side of the same coin.

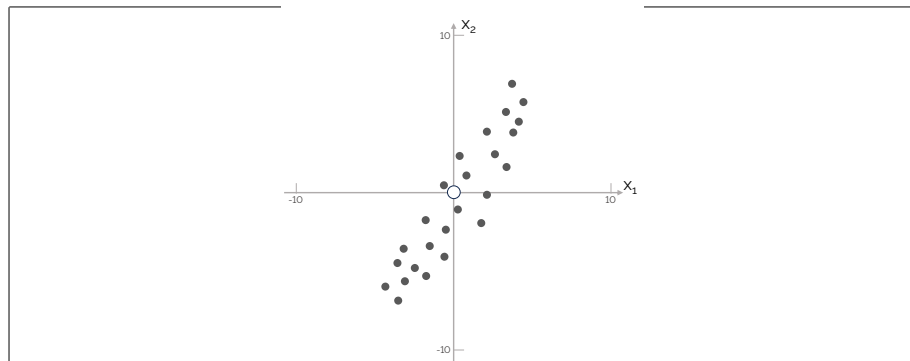


Figure 1.9. Original observations of a two-dimension dataset, x_1 and x_2 .

Indeed, PCA also looks for properties that allow reconstructing the original features as accurately as possible. In practice, it aims at minimizing the total reconstruction error that is the average squared distance between the original observations and their respective projection.

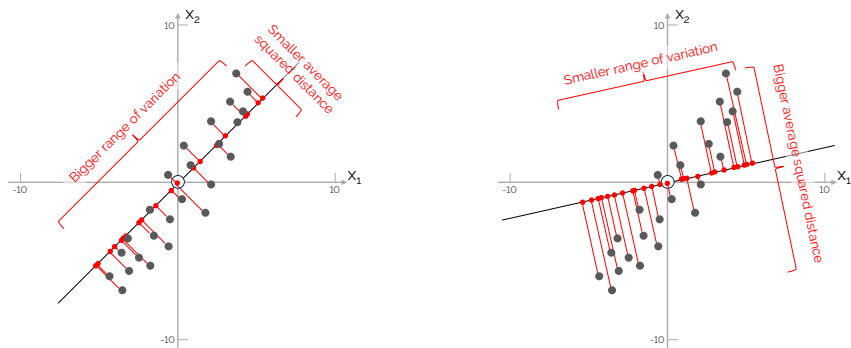


Figure 1.10. Two different projections (red dots) of the original observations (grey dots). Projection on the left captures a bigger variance than the projection on the right. At the same time, the average squared distance between the original observations and their respective projection is smaller for the projection on the left. Consequently, the left projection is closer to be the first PC than to the right projection.

More mathematically, the first principal component (PC), z_1 , is then a linear function, $\alpha_1^T \mathbf{x}$, of the different variables of \mathbf{x} with maximum variance:

$$z_1 = \sum_{j=1}^p \alpha_{1j} x_j = \boldsymbol{\alpha}_1^T \mathbf{x} = \alpha_{11} x_1 + \alpha_{12} x_2, \quad (1.25)$$

where T means the transpose vector. Then, $z_2 = \boldsymbol{\alpha}_2^T \mathbf{x}$, is another linear function of \mathbf{x} , uncorrelated with z_1 and maximizing the variance. These linear transformations can be seen as projection of the original data on the principal direction, i.e. PCs (see Figure 1.11). In more general cases, one can write $z_k = \boldsymbol{\alpha}_k^T \mathbf{x}$ as the k^{th} PC. There can be up to p PCs even though, usually, most of the variance of the original data can be captured by m PCs where $m \ll p$. The interested reader is invited to refer to the work of Jolliffe [50] for further mathematical demonstrations, information and examples.

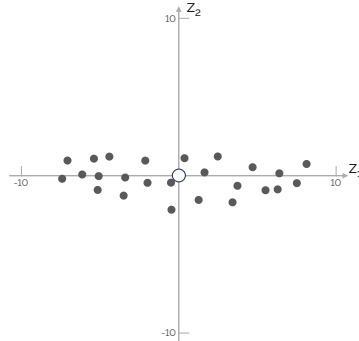


Figure 1.11. Projection of the original observations with respect to their PCs. The variation of the realisations was more significant in the direction of x_2 than x_1 . Once projected with respect to their PCs, the variation is even more significant in the direction of z_1 than in either of the original variables, as it captures most of their variance.

1.4.2 Principal components of the transition

As introduced, the objective is to define the main technological drivers of the variation through the transition to 2050 subject to uncertainties. To do so, before calculating the PCs of the transition, three preliminary steps are necessary: (i) selection of the right data, (ii) data scaling and, (iii) outliers management. Like any other dimension-reduction process, PCA has to be supplied with relevant data to reach the stated objective. Like the normalization of the eigenvectors (see Section 1.4.1), data scaling is fundamental to compare features having potentially different units and/or order of magnitude. Finally, properly handling the outliers allows reaching the relevant level of metric between the too vague information of the sole total transition cost and too

many details hidden in the peculiar/outlying cases. After this preprocessing, PCs can be computed for each of the year of the transition then aggregated to give a bigger picture over the whole transition.

Data selection

To characterize the variations of design within the transition under uncertainties, we have focused on the installed capacities, $\mathbf{F}(y, j)$ for all $y \in YEARS$ and $j \in TECH$ (see Eq. 1.13). Even though these represent only the design part of the result of the optimization, along with the operation, focusing on the installed capacities give a direct information regarding the required capital investment (see Eq. ??) and, more indirectly, the resources to use. In other words, it captures the technological landscape of the transition. Having defined the type of variable to consider, we need to assemble a relevant dataset. This is given by the runs to quantify the impact of the uncertain parameters on the total cost of transition required by the method described in Section 1.2. Overall, the original dataset is $\mathbf{x}(y, j, s)$ where, on top of y and j previously defined, $s \in [1, 2, \dots, S]$ stands for the sample number of the uncertainty quantification method. For the investigated case detailed in Chapter ??, this represents $S = 1260$ samples resulting from the perfect foresight optimization of the transition pathway under uncertainties. Finally, among the seven representative years of the transition, we do not consider 2020 as it is the initialisation year for which the design of the system is fixed, to be representative of the actual design that was in place (see Appendix ??). In other words, we focus here only on the years 2025, 2030, 2035, 2040, 2045 and 2050. This gives the whole dataset considered in this PCA (see Figure 1.12). Appendix A.3 gives the distribution of the installed capacities among the different end-use sectors from the GSA.

Data scaling

Preprocessing the dataset before employing a method to reduce dimensionality, like PCA, can greatly affect the structure of the simplified representation and the characteristics of the features extracted from the dataset [52, 53]. Scaling the original raw data via normalization, i.e. reducing data to $[0, 1]$ interval has a double purposes: to assess variables (i) representing different sorts of features, with different units (e.g. installed capacity of electricity and mobility technologies) and, (ii) ranging over the different orders of magnitude (e.g. installed capacity of private and public mobility) (see Appendix ??). Consequently, the first part of this data preprocessing consists in scaling the installed capacities versus their respective sector and representative year (see Eq.

Sample _s	TECH ₁	TECH ₂	TECH ₃	...	TECH _p
2025					
2030					
Sample ₂	TECH ₁	TECH ₂	TECH ₃	...	TECH _p
Sample ₁	TECH ₁	TECH ₂	TECH ₃	...	TECH _p
2025	F _{1,2025}	F _{2,2025}	F _{3,2025}	...	F _{p,2025}
2030	F _{1,2030}	F _{2,2030}	F _{3,2030}	...	F _{p,2030}
2035	F _{1,2035}	F _{2,2035}	F _{3,2035}	...	F _{p,2035}
2040	F _{1,2040}	F _{2,2040}	F _{3,2040}	...	F _{p,2040}
2045	F _{1,2045}	F _{2,2045}	F _{3,2045}	...	F _{p,2045}
2050	F _{1,2050}	F _{2,2050}	F _{3,2050}	...	F _{p,2050}

Figure 1.12. Original raw data considered in the Principal Component Analysis (PCA) of the variation of the design strategy through the transition, $\mathbf{x}(y, j, s)$, accounting for the p possible technologies to install.

1.26). The sectors, as defined in EnergyScope, are the electricity, high-temperature (HT) heat, low-temperature (LT) heat, passenger mobility, freight mobility, non-energy demand (NED), storage and infrastructures. For instance, the installed capacity of PV panels in the year y of the sample s is scaled by the maximum installed capacity in the electricity sector in the year y among all the samples.

$$\mathbf{x}^*(y, j, s) = \frac{\mathbf{x}(y, j, s)}{\max_{sec,y}(\mathbf{x}(y, j, s))} \quad \forall y \in YEARS, sec \in SECTORS \quad (1.26)$$

Then, to give “directions/metrics” representative to the size of each sector within the energy system, we added another weight based on the relative share of commodity produced by each sector. For the case study of Belgium detailed in Chapter ??, this gives a higher weight for electricity and low-temperature heat sectors (see Figure 1.13).

To do so, we have arbitrarily considered these shares from the REF case, where the pathway is optimized according to the perfect foresight approach and considering all the uncertain parameters to their nominal value (see Chapter ??). The end-use-demands as well as the commodity produced for the sector coupling are based on the results of this deterministic REF case. For instance, the share of the electricity sector accounts for its EUD and the electricity produced to supply other sectors (e.g. heat, mobility). Finally, to compare apples with apples, we converted the EUD in the mobility sectors, i.e. passenger and freight, into the final energy consumed (FEC) they require in the REF case. This gives the second weighing factor to scale data, on top of the one of Eq. 1.26 (see Eq. 1.27).

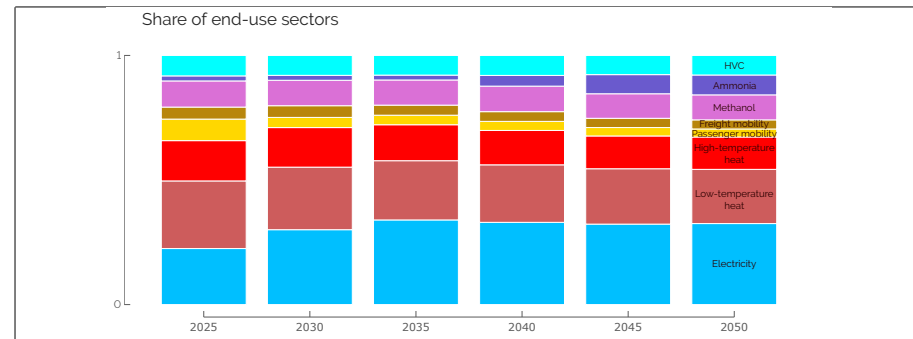


Figure 1.13. Multiplying factor for each of the end-use sectors in the case of Belgian energy transition. These shares are based on results of the reference scenario (REF) where nominal values are considered for the uncertain parameters and the transition is optimized through the perfect foresight approach. Over the transition, sectors like electricity (i.e. from 22% in 2025 to 33% in 2050) or ammonia (i.e. from 2% to 8%) become more important due to sector coupling, e.g. e-mobility or ammonia-CCGT.

$$\mathbf{x}^{**}(y, j, s) = \mathbf{x}^*(y, j, s) \cdot \text{share}_{\text{EUD}}(y, sec) \quad \forall y \in \text{YEARS}, sec \in \text{SECTORS} \quad (1.27)$$

One would notice that this second scaling factor omits the infrastructure and storage technologies. In the process to define “metrics” to assess the robustness of a policy for the case of Belgium, this has a negligible impact. Indeed, the variation of the installed capacity of these technologies are either limited compared to end-use-type (EUT) technologies, i.e. limiting their influence in the definition of PCs, or directly linked to these EUT technologies (e.g. district heating network (DHN) installed capacity is directly proportional to technologies producing LT heat in DHN or the additional capacity of grid is caused by additional capacities of VRES).

Outliers management

Handling outliers is one of the biggest challenges in data science [54]. These are defined as data points differing significantly from the rest of the data set. Being extreme values, outliers influence the overall dataset variance and, consequently, rotate the PCs directions towards them [55]. In the context of PCA, outliers could be defined as “model fit outliers” as their presence influences the fit of the model. There are several techniques to detect/define and handle the

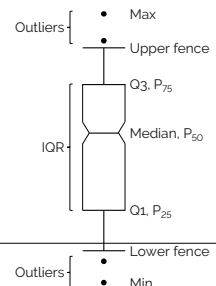


Figure 1.14

outliers [54]. In this work, detection is performed via the box plot technique, as outliers are identified as those points lying beyond the plot's whiskers, or fences. These whiskers are themselves constructed as being 1.5 times the interquartile range (IQR) ($Q_3 - Q_1$) higher or lower than the third (Q_3) or first quartile (Q_1), respectively (see Figure 1.14). Therefore, the installed capacity of a technology in the year y of the sample s is defined as an outlier if it falls out of this range compared to the rest of the dataset for this specific technology and year across all the samples. There exist several techniques to handle these outliers depending on their nature or the method used to identify them. Since all the data points correspond to a result provided by the optimization, we have decided to keep these points but carry out a modification of them [54]. In practice, the value of “high outliers” or “low outliers” is set to the upper or lower fence, respectively. In practice, this modification narrows the variation range of features presenting outliers and, consequently, reduces their weight in the different PCs.

Principal components of each representative year

Now that data are selected and preprocessed, principal components are first computed for each representative year separately, using the Python package PCA from SKLEARN.DECOMPOSITION. As explained in Section 1.4.1, the number of PCs per year to retain can go up to the number of considered variables (i.e. 73⁴ in our case study) which is intractable. Moreover, the first PCs keep track of most of the variance of the system whereas the last ones present a smaller interest. Choosing the appropriate threshold involves a trade-off. Retaining too few principal components may result in loss of important information, while retaining too many may lead to unclear analysis. In this work is to compute, for each of the representative years of the transition (except 2020), the PCs capture 90% of the total variance of this year [50]. At the end of this step, we have a list of m PCs, i.e. $\text{PC}_{y,i}$ where y stands for the year between 2025 and 2050 and

$$\sum_{i=0}^m \text{var}(\text{PC}_{y,i}) \geq 90\% \sum_{i=0}^p \text{var}(\text{PC}_{y,i}) \quad \forall y \in \text{YEARS}, \quad (1.28)$$

where m is presumably different for each representative year and p is the total number of variables, hence the maximum number of PCs. For the entire transition, it gives a

⁴73 technologies out of the 113 in total as we do not consider the 15 infrastructure technologies nor the 25 storage technologies.

total of M $\text{PC}_{y,i}$.

Principal components of the transition

The final step consists in defining metrics on the whole transition based on the $\text{PC}_{y,i}$ computed for each representative year, separately. To do so, all the $\text{PC}_{y,i}$ from every year are sorted together in a descending order based on their respective variance. Then, starting with the one with the highest absolute variance, all the other $\text{PC}_{y,i}$ similar to it are clustered together. The similarity between two PCs is defined according to the cosine similarity approach, especially appropriate in high-dimensional positive spaces [56]. Indeed, as detailed in Section 1.4.1, a PC represents a vector for which the components are related to each variable of interest. Therefore, in this work, PCs are considered similar if their cosine similarity, $S_C(A, B)$, is either greater or equal to 90% or lower or equal to -90% (see Eq. 1.29). It is important to consider the second specific case as PCA gives the magnitude of variation within the original feature space via the components of the eigenvectors, regardless of the direction of these vectors. For instance, in a two-dimension original space, if the first PC has $(\sqrt{2}/2; \sqrt{2}/2)$ as eigenvector, this could be $(-\sqrt{2}/2; -\sqrt{2}/2)$. The second vector being the opposite of the first, they are considered as equivalent in the regard of PCA.

$$S_C(A, B) := \cos(\theta) = \frac{\mathbf{A} \cdot \mathbf{B}}{\|\mathbf{A}\| \|\mathbf{B}\|} = \frac{\sum_{i=1}^n A_i B_i}{\sqrt{\sum_{i=1}^n A_i^2} \cdot \sqrt{\sum_{i=1}^n B_i^2}} \geq 90\% \text{ or } \leq -90\%, \quad (1.29)$$

where A and B represent two different PCs. The components of these similar PCs are then averaged to form the first PC of the transition, $\text{PC}_{\text{transition},1}$. Then, the process repeats with the $\text{PC}_{y,i}$ with the highest absolute variance but that has not been integrated in the construction of $\text{PC}_{\text{transition},1}$, to form $\text{PC}_{\text{transition},2}$. This goes on until the sum of the absolute variance of the N $\text{PC}_{y,i}$ used to construct these $\text{PC}_{\text{transition}}$ is greater or equal to $\alpha\%$ of the sum of the absolute variance of all the M $\text{PC}_{y,i}$, i.e. the “total transition variance”, generated at the previous step:

$$\sum_{i=0}^N \text{var}(\text{PC}_{y,i}) \geq \alpha\% \sum_{i=0}^M \text{var}(\text{PC}_{y,i}) \quad (1.30)$$

In our case, we have decided to set the value of α to 80% as, beyond this value, the marginal gain of captured variance becomes too “costly” with regard to the number of

PC_y , i.e. the level of details, to account for (see Figure 1.15). For instance, capturing up to 90% of the total transition variance would mean almost doubling the number of PC_y to consider and, consequently, the number of directions of variation to assess.

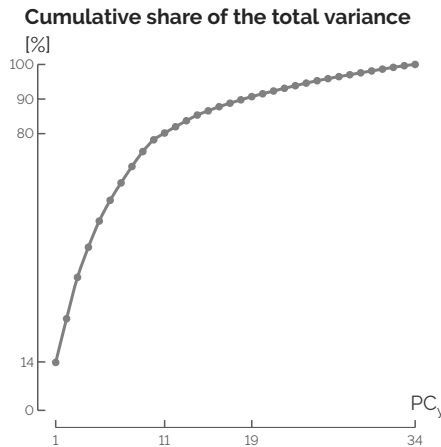


Figure 1.15. Cumulative share of the sum of the transition variance versus the number of PC_y . Passing a certain threshold, here 80%, the number of PC_y to consider increase significantly compared to the share of transition variance that they capture.

Robustness assessment of roadmaps

Similarly to the work of Moret et al. [19], roadmaps are defined by setting minimal installed capacities based on the results of different transition pathway optimizations (see Chapter 2). The $PC_{transition}$ are the “direction/metrics” on which are projected the results from the myopic pathway optimization subject to minimal installed capacities set by these roadmaps. In conclusion, a roadmap would be defined as more robust than another one if the projection of its myopic runs on the different $PC_{transition}$ spans on a more narrow range (see Figure 1.16). The bounds of this “range of projection” are computed as the mean, μ , of the projected data \pm a 95% confidence level, CL, on the margin of error, MOE:

$$\text{range of projection} = [\mu - \text{MOE}; \mu + \text{MOE}],$$

where the margin of error, MOE, is computed thanks to standard error of the mean, SEM, and assuming a Student’s, distribution, t, of the N projected data:

$$\text{MOE} = \text{SEM} \cdot \text{PPF}_t((1 + \text{CL})/2, N - 1),$$

where PPF_t is the percent point function (i.e. inverse of cumulative distribution function) of the Student's distribution.

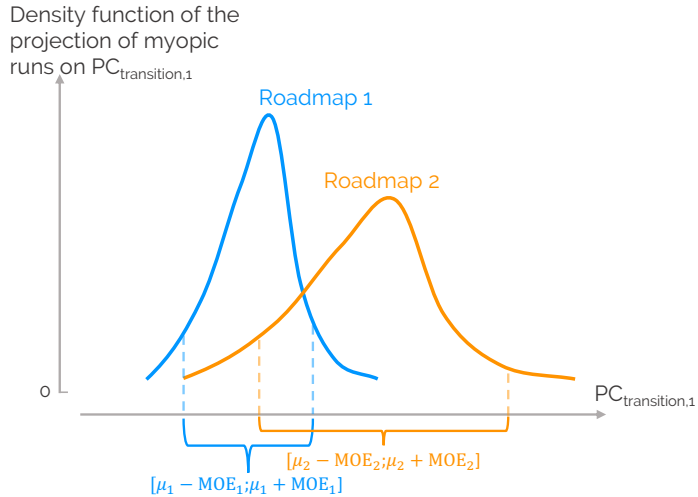


Figure 1.16. Projection on the first PC of the transition, $\text{PC}_{\text{transition},1}$, of the different myopic runs under uncertainties based on different roadmaps. Given that the distribution resulting from roadmap 1 spans over a more narrow range of this PC of the transition, we conclude that this roadmap is more robust than roadmap 2 according to the direction of variation described by $\text{PC}_{\text{transition},1}$.

Chapter 2

Robustness assessment of pathway roadmaps

“The more data we have, the more likely we are to drown in it.”

Nassim Nicholas Taleb, in *Fooled by Randomness: The Hidden Role of Chance in Life and in the Markets*, 2008

Assessing the robustness of a roadmap driving the transition pathway of a whole-energy system is complex, especially due to the curse of dimensionality. This curse comes from the number of variables of the system (e.g. the installed capacity of technologies), the multiple-year approach specific to the pathway optimisation (i.e. versus the snapshot approach) or the number of uncertain parameters. On top of this, the sector coupling interconnecting the installed capacities and the used resources among the different (non-)energy sectors can make harder the understanding of big trends of such a system. To navigate through this load of uncertain and interconnected data, it is necessary to assess the robustness of pathway roadmaps.

To deal with such uncertainties, decision-makers have several options: (i) resistance; (ii) resilience; (iii) static robustness; and (iv) adaptive robustness [57]. Where resistance consists in planning for the worst-case scenario, resilience aims at a fast recovery whatever the conditions in the future. Finally, in static robustness, one seeks for a roadmap that would perform “satisfactorily” in a wide range of plausible futures, whereas, a roadmap would be dynamically robust if it is prepared to adapt in case of a change in conditions. Where the adaptability of the policy was addressed in Chapter ??, the objective of this chapter is to apply the method described in Section 1.4 to deal with the static robustness of pathway roadmaps. Castrejon-Campos et al. [58] assessed

policy mix following the same philosophy of “satisfactory level of performance” as [57]. In their work, they mostly focused on the electricity sector, accounting for a variety of stakeholders and related interests using STET (Socio-Technical Energy Transition) models to capture more properly societal and behavioral aspects in relation with policy implementation, enriching purely techno-economy model, like EnergyScope, that usually assume rational choice within an overall cost minimization. However, in the case of the transition pathway of a whole-energy system, the challenges stand here in the definition of the “performance metric” as well as the “satisfactory level of performance”. Between the sole total transition cost and the entire set of installed technologies that give too few and too much information, respectively, the performance metric here is defined through the PCA approach. Then, when comes the “satisfactory level of performance”, we propose a relative level of performance through a comparative analysis of different roadmaps. In other terms, one roadmap will not be robust or not in itself but rather more or less robust than another one.

Contributions

The main contributions of this chapter is the application of the methodology proposed in Section 1.4 to the case study of the Belgian energy transition. First, we develop the different steps that lead to the principal components of the transition. We analyse these big trends of variation and highlight the fact that these variations stand for the entire pathway, a group of consecutive representative years or rather on a tipping-year. Then, and most importantly, we assess the robustness of different technological roadmaps by projecting their resulting myopic pathway against these directions of variation. The application of PCA to provide a new metric for robustness applied to the case of Belgium is the added-value of this chapter.

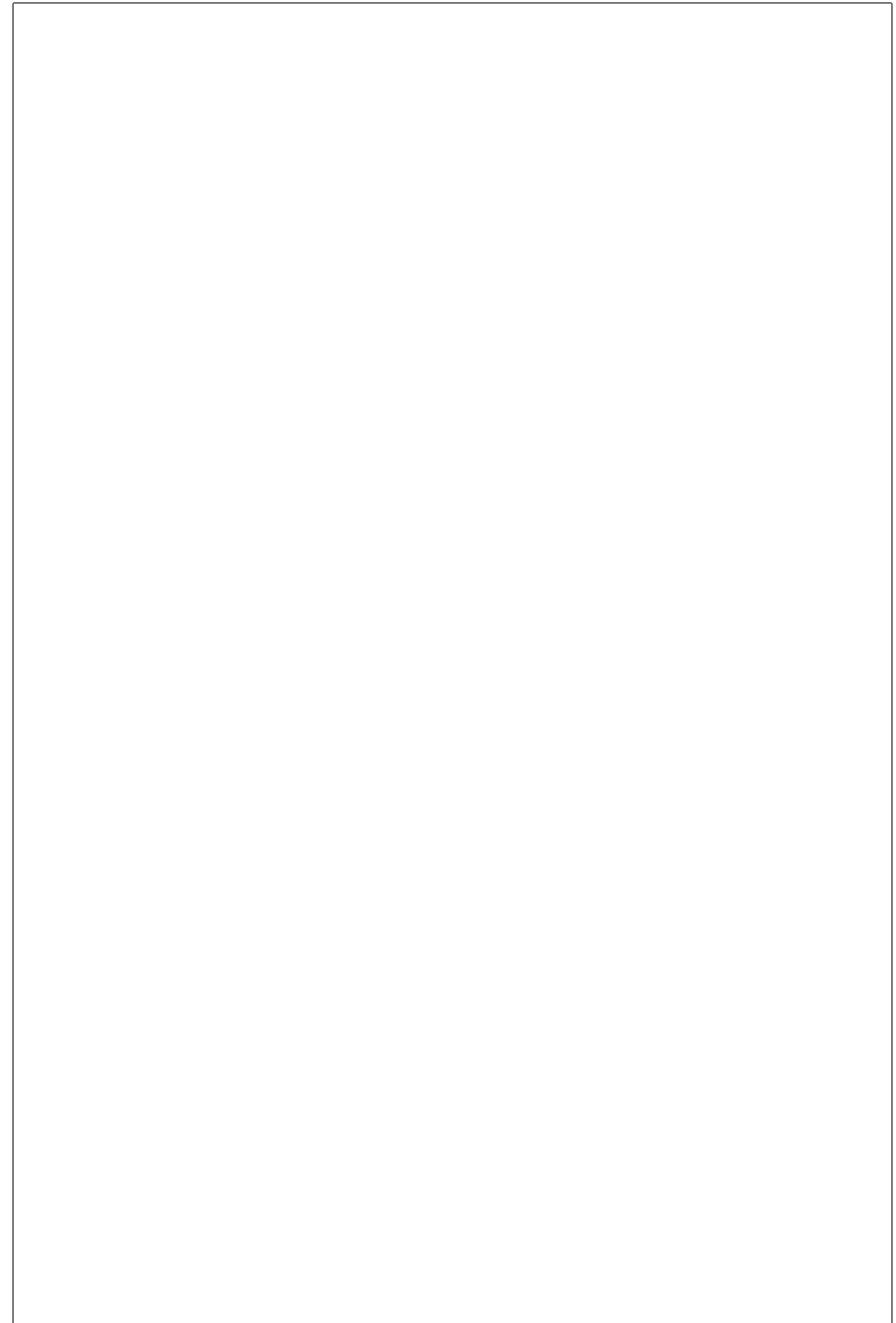
2.1 Definition of the principal components of the transition

As detailed in Section 1.4.2, we have decided to define the directions of variation, i.e. the robustness metrics, based on the installed capacities through the transition in the different end-use sectors, i.e. electricity, HT heat, LT heat, passenger mobility, freight mobility, high value chemicals (HVC), ammonia and methanol. These capacities represent the technological roadmaps to supply these EUD while respecting the CO₂-budget. As introduced in Section 1.4.2, the data considered in this method come from the GSA carried out on the perfect foresight optimisation of the Belgian transition pathway (see Chapter ??). This gave 1260 different transitions resulting, for each

of them, from the pathway optimisation subject to a sample of uncertain parameters (see Section 1.2.1). Appendix A.3 gives the exhaustive distributions of the installed capacities among the different end-use sectors from the GSA.

2.1.1 Principal components of each representative year

After the pre-preprocessing of the raw data (i.e. data scaling and outliers management, see Section 1.4.2), the principal components (PCs) of each representative year of the transition, except 2020 as the initialisation year, can be computed



Bibliography

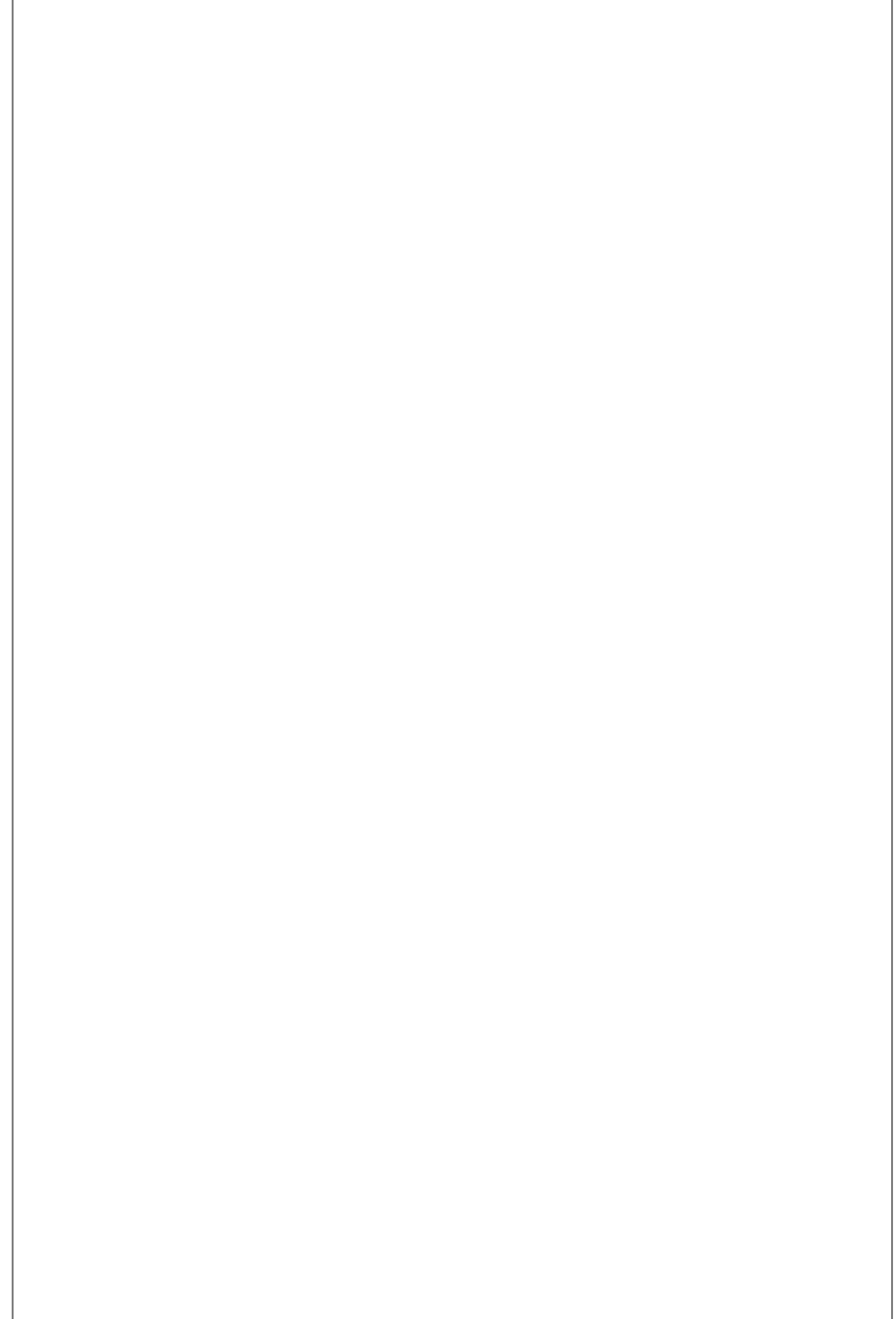
- [1] G. Limpens, Generating energy transition pathways: application to Belgium, Ph.D. thesis, Université Catholique de Louvain, 2021.
- [2] S. Babrowski, T. Heffels, P. Jochem, W. Fichtner, Reducing computing time of energy system models by a myopic approach: A case study based on the perseus-net model, *Energy systems* 5 (2014) 65–83.
- [3] E. Guevara, F. Babonneau, T. Homem-de Mello, Modeling uncertainty processes for multi-stage optimization of strategic energy planning: An auto-regressive and markov chain formulation (2022).
- [4] S. Moret, V. Codina Gironès, M. Bierlaire, F. Maréchal, Characterization of input uncertainties in strategic energy planning models, *Applied Energy* 202 (2017) 597–617.
- [5] G. Limpens, D. Coppitters, X. Rixhon, F. Contino, H. Jeanmart, The impact of uncertainties on the Belgian energy system: Application of the Polynomial Chaos Expansion to the EnergyScope model, *Proceedings of the ECOS* (2020).
- [6] X. Rixhon, G. Limpens, D. Coppitters, H. Jeanmart, F. Contino, The role of electrofuels under uncertainties for the Belgian energy transition, *Energies* 14 (2021) 4027.
- [7] B. Goffaux, Pathway towards energy sustainability in Belgium under uncertainties, 2021. URL: <https://dial.uclouvain.be/memoire/ucl/object/thesis:30574>.
- [8] S. Moret, M. Bierlaire, F. Maréchal, Strategic energy planning under uncertainty: a mixed-integer linear programming modeling framework for large-scale energy systems, in: *Computer Aided Chemical Engineering*, volume 38, Elsevier, 2016, pp. 1899–1904.
- [9] G. Limpens, S. Moret, H. Jeanmart, F. Maréchal, EnergyScope TD: A novel open-source model for regional energy systems, *Applied Energy* 255 (2019) 113729.
- [10] G. Limpens, X. Rixhon, F. Contino, H. Jeanmart, Energyscope pathway: an open-source model to optimise the energy transition pathways of a regional whole-energy system, Elsevier in *Applied Energy* 358 (2024). doi:<https://doi.org/10.1016/j.apenergy.2023.122501>.

- [11] D. Coppitters, Robust design optimization of hybrid renewable energy systems, Vrije Universiteit Brussel (VUB), University of Mons (UMONS), Mons (2021).
- [12] M. Geidl, P. Favre-Perrod, B. Klöckl, G. Koeppl, A greenfield approach for future power systems, Proc. of Cigre General Session 41 (2006) 136.
- [13] G. Limpens, EnergyScope Pathway documentation, Accessed 2022. URL: <https://energyscope-pathway.readthedocs.io/en/v1.1/>.
- [14] T. Stocker, Climate change 2013: the physical science basis: Working Group I contribution to the Fifth assessment report of the Intergovernmental Panel on Climate Change, Cambridge university press, 2014.
- [15] J. Schnidrig, J. Brun, F. Maréchal, M. Margni, Integration of life cycle impact assessment in energy system modelling, Proceedings of ECOS 2023 (2023).
- [16] K. Poncelet, E. Delarue, D. Six, W. D'haeseleer, Myopic optimization models for simulation of investment decisions in the electric power sector, in: 2016 13th International Conference on the European Energy Market (EEM), IEEE, 2016, pp. 1–9.
- [17] F. F. Nerini, I. Keppo, N. Strachan, Myopic decision making in energy system decarbonisation pathways. a uk case study, Energy strategy reviews 17 (2017) 19–26.
- [18] C. F. Heuberger, I. Staffell, N. Shah, N. Mac Dowell, Impact of myopic decision-making and disruptive events in power systems planning, Nature Energy 3 (2018) 634–640.
- [19] S. Moret, F. Babonneau, M. Bierlaire, F. Maréchal, Overcapacity in european power systems: Analysis and robust optimization approach, Applied Energy 259 (2020) 113970.
- [20] AMPL Optimization Inc., AMPL Python API, <https://amplpyAMPL.com/en/latest/>, 2024.
- [21] V. Krey, Vergleich kurz-und langfristig ausgerichteter optimierungsansätze mit einem multi-regionalen energiesystemmodell unter berücksichtigung stochastischer parameter (2006).
- [22] X. Yue, S. Pye, J. DeCarolis, F. G. Li, F. Rogan, B. Ó. Gallachóir, A review of approaches to uncertainty assessment in energy system optimization models, Energy strategy reviews 21 (2018) 204–217.
- [23] G. Mavromatidis, K. Orehounig, J. Carmeliet, Uncertainty and global sensitivity analysis for the optimal design of distributed energy systems, Applied Energy 214 (2018) 219–238.
- [24] J. Peace, J. Weyant, Insights not numbers: the appropriate use of economic models, White paper of Pew Center on Global Climate Change (2008).

- [25] C. Marnay, A. S. Siddiqui, Addressing an uncertain future using scenario analysis, Lawrence Berkeley National Laboratory, 2006.
- [26] X. Li, S. Moret, F. Baldi, F. Maréchal, Are renewables really that expensive? the impact of uncertainty on the cost of the energy transition, in: Computer Aided Chemical Engineering, volume 46, Elsevier, 2019, pp. 1753–1758.
- [27] D. Coppitters, W. De Paepe, F. Contino, Robust design optimization of a photovoltaic-battery-heat pump system with thermal storage under aleatory and epistemic uncertainty, Energy 229 (2021) 120692.
- [28] Climact, VITO, New scenarios for a climate neutral Belgium by 2050, Technical Report, 2021. URL: <https://klimaat.be/doc/climate-neutral-belgium-by-2050-report.pdf>.
- [29] Hydrogen Import Coalition, Shipping sun and wind to Belgium is key in climate neutral economy, <https://www.portofantwerp.com/sites/default/files/Hydrogen%20Import%20Coalition.pdf>, 2021.
- [30] D. Coppitters, W. De Paepe, F. Contino, Robust design optimization and stochastic performance analysis of a grid-connected photovoltaic system with battery storage and hydrogen storage, Energy 213 (2020) 118798.
- [31] D. Coppitters, P. Tsirikoglou, W. D. Paepe, K. Kyprianidis, A. Kalfas, F. Contino, RHEIA: Robust design optimization of renewable Hydrogen and dErIved energy cArrier systems, Journal of Open Source Software 7 (2022) 4370. doi:10.21105/joss.04370.
- [32] D. Coppitters, RHEIA documentation, Accessed 2022. URL: <https://rheia.readthedocs.io/en/latest/index.html>.
- [33] B. Sudret, Polynomial chaos expansions and stochastic finite element methods, Risk and reliability in geotechnical engineering (2014) 265–300.
- [34] P. Bratley, B. Fox, Implementing sobols quasirandom sequence generator (algorithm 659), ACM Transactions on Mathematical Software 29 (2003) 49–57.
- [35] M. D. Morris, Factorial Sampling Plans for Preliminary Computational Experiments, Technometrics 33 (1991) 161–174.
- [36] G. Sin, K. V. Gernaey, Improving the morris method for sensitivity analysis by scaling the elementary effects, in: Computer Aided Chemical Engineering, volume 26, Elsevier, 2009, pp. 925–930.
- [37] S. Moret, Strategic energy planning under uncertainty, Ph.D. thesis, EPFL, 2017.

- [38] P. Turati, N. Pedroni, E. Zio, Simulation-based exploration of high-dimensional system models for identifying unexpected events, *Reliability Engineering and System Safety* 165 (2017) 317–330.
- [39] D. Cao, W. Hu, J. Zhao, G. Zhang, B. Zhang, Z. Liu, Z. Chen, F. Blaabjerg, Reinforcement learning and its applications in modern power and energy systems: A review, *Journal of modern power systems and clean energy* 8 (2020) 1029–1042.
- [40] R. S. Sutton, A. G. Barto, *Reinforcement learning: An introduction*, MIT press, 2018.
- [41] David Silver, RL Course by David Silver, <https://www.youtube.com/watch?v=2pWv7G0vuf0&list=PLzvuYNsE1EZAXYR4FJ75jcJseBmo4KQ9->, 2016.
- [42] A. Perera, P. Kamalaruban, Applications of reinforcement learning in energy systems, *Renewable and Sustainable Energy Reviews* 137 (2021) 110618.
- [43] T. Haarnoja, A. Zhou, P. Abbeel, S. Levine, Soft actor-critic: Off-policy maximum entropy deep reinforcement learning with a stochastic actor, in: *International conference on machine learning*, PMLR, 2018, pp. 1861–1870.
- [44] T. Haarnoja, H. Tang, P. Abbeel, S. Levine, Reinforcement learning with deep energy-based policies, in: *International conference on machine learning*, PMLR, 2017, pp. 1352–1361.
- [45] B. D. Ziebart, Modeling purposeful adaptive behavior with the principle of maximum causal entropy, Carnegie Mellon University, 2010.
- [46] A. Raffin, A. Hill, A. Gleave, A. Kanervisto, M. Ernestus, N. Dormann, Stable-baselines3: Reliable reinforcement learning implementations, *The Journal of Machine Learning Research* 22 (2021) 12348–12355.
- [47] M. Abadi, A. Agarwal, P. Barham, E. Brevdo, Z. Chen, C. Citro, G. S. Corrado, A. Davis, J. Dean, M. Devin, et al., Tensorflow: Large-scale machine learning on heterogeneous distributed systems, *arXiv preprint arXiv:1603.04467* (2016).
- [48] K. Pearson, On lines and planes of closest fit to systems of points in space., *The London, Edinburgh, and Dublin philosophical magazine and journal of science* 2 (1901) 559–572.
- [49] H. Hotelling, Analysis of a complex of statistical variables into principal components., *Journal of educational psychology* 24 (1933) 417.
- [50] I. T. Jolliffe, *Principal component analysis for special types of data*, Springer, 2002.
- [51] K. Zdybał, G. D'Alessio, G. Aversano, M. R. Malik, A. Coussement, J. C. Sutherland, A. Parente, Advancing reacting flow simulations with data-driven models, *arXiv preprint arXiv:2209.02051* (2022).

- [52] A. Parente, J. C. Sutherland, Principal component analysis of turbulent combustion data: Data pre-processing and manifold sensitivity, *Combustion and flame* 160 (2013) 340–350.
- [53] K. Peerenboom, A. Parente, T. Kozák, A. Bogaerts, G. Degrez, Dimension reduction of non-equilibrium plasma kinetic models using principal component analysis, *Plasma Sources Science and Technology* 24 (2015) 025004.
- [54] H. Aguinis, R. K. Gottfredson, H. Joo, Best-practice recommendations for defining, identifying, and handling outliers, *Organizational research methods* 16 (2013) 270–301.
- [55] I. Stanimirova, M. Daszykowski, B. Walczak, Dealing with missing values and outliers in principal component analysis, *Talanta* 72 (2007) 172–178.
- [56] P. Xia, L. Zhang, F. Li, Learning similarity with cosine similarity ensemble, *Information sciences* 307 (2015) 39–52.
- [57] W. E. Walker, R. J. Lempert, J. H. Kwakkel, Deep uncertainty, *Delft University of Technology* 1 (2012).
- [58] O. Castrejon-Campos, L. Aye, F. K. P. Hui, Making policy mixes more robust: An integrative and interdisciplinary approach for clean energy transitions, *Energy Research & Social Science* 64 (2020) 101425.
- [59] SPF Economie, Vision and strategy hydrogen, October 2022. URL: <https://economie.fgov.be/sites/default/files/Files/Energy/View-strategy-hydrogen.pdf>.



Appendix A

Pathway optimisation under uncertainties

A.1 Total transition cost

Table A.1 gives the ranking and total Sobol index over the total transition cost of each of the 34 parameters listed in ???. The first column shows these indicators for the GSA applied on the hourly pathway model. For information, the second column gives the same indicators but for an uncertainty quantification carried out on the monthly pathway model that has some limitations [10] but has the main advantage to run much faster. Given the similar rankings of the parameters between these two, this comparison shows that the monthly model can be a computationally efficient proxy to quantify the uncertainties of the actual hourly model and point out the key parameters on optimisation-driving objective, the total transition cost.

Besides the top-4 parameters, rankings are slightly different. The main difference in terms of ranking relates to the import of electricity from abroad, i.e. its cost of purchasing and its availability. Indeed, as observed by Limpens et al. [10], the monthly model does not require this import given the easier integration of monthly-averaged local VRES. However, this does not jeopardize the comparative analysis given the similar Sobol' indices. Given their wide range of uncertainty [-64.3%; 179.8%] and their significant role to meet the CO₂-budget, the cost of purchasing electrofuels is the first, by far, impacting parameter. Next, comes, naturally, the industrial EUD, representing, at the nominal value, 60% of the total demands by 2050. The top-3 is completed by the variation of the interest rate, directly impacting the annualisation and the salvage values of the assets. Finally, since the current Belgian whole-energy system deeply

relies on fossil resources, and would still do in the near future, the cost of purchasing fossil fuels is part of the impacting parameters. On the contrary, due to the very low annualised, cost, long lifetime leading to a significant salvage value and a low-emitting fuel, the parameters related to SMR barely impact the total transition cost.

Table A.1. Total Sobol' indices of the uncertain parameters over the total transition cost in the monthly and hourly pathway models. The similar rankings (and indices) show the validity of using the faster (even though less accurate) monthly model to assess uncertainties over the hourly model.

Parameter	Ranking (Sobol' index)	
	Hourly model	Monthly model
Purchase electrofuels	1 (46.8%)	1 (47.4%)
Industry EUD	2 (23.2%)	2 (23.5%)
Interest rate	3 (12.0%)	3 (11.0%)
Purchase fossil fuels	4 (5.7%)	4 (6.9%)
Variable OPEX of technologies	5 (3.1%)	5 (2.9%)
Purchase biofuels	6 (2.6%)	6 (2.6%)
CAPEX electric motor	7 (2.1%)	8 (1.9%)
Purchase electricity	8 (1.5%)	34 (<0.1%)
Hourly load factor wind turbines	9 (1.1%)	9 (1.3%)
Hourly load factor PV	10 (1.1%)	7 (1.9%)
Potential capacity SMR	11 (0.9%)	11 (0.9%)
CAPEX car	12 (0.8%)	13 (0.7%)
Available local biomass	13 (0.7%)	12 (0.8%)
Passenger mobility EUD	14 (0.7%)	14 (0.7%)
Modal share change LT-heat	15 (0.5%)	15 (0.5%)
Max capacity PV	16 (0.5%)	10 (1.1%)
Households EUD	17 (0.5%)	16 (0.5%)
Services EUD	18 (0.5%)	17 (0.4%)
Max share of public transport	19 (0.3%)	19 (0.3%)
Max capacity onshore wind	20 (0.3%)	18 (0.3%)
CAPEX PV	21 (0.2%)	20 (0.2%)
Efficiency electric motor	22 (0.2%)	22 (0.1%)
Max capacity offshore wind	23 (0.2%)	21 (0.2%)
Available electricity import	24 (0.1%)	33 (<0.1%)
CAPEX ICE	25 (0.1%)	24 (0.1%)
CAPEX fuel cell engine	26 (0.1%)	23 (0.1%)
Efficiency fuel cell engine	27 (0.1%)	25 (<0.1%)
Modal share change freight mobility	28 (0.1%)	26 (<0.1%)
Modal share change passenger mobility	29 (<0.1%)	27 (<0.1%)
CAPEX grid reinforcement	30 (<0.1%)	30 (<0.1%)
CAPEX efficiency measures	31 (<0.1%)	28 (<0.1%)
CAPEX bus	32 (<0.1%)	29 (<0.1%)
CAPEX SMR	33 (<0.1%)	32 (<0.1%)
CAPEX power grid	34 (<0.1%)	31 (<0.1%)

A.2 Imported renewable electrofuels

Table A.2. Comparison of the quantities of imported renewable electrofuels, in TWh, between the REF case, the SMR case and the statistical features from the GSA (i.e. Q1, median and Q3). 2020 is not in the table as, per assumption, no renewable electrofuel is imported for this year. For the sake of clarity, zeroes are replaced by “-”.

Year	Case	e-methane	e-hydrogen	e-ammonia	e-methanol
2025	REF	-	-	10	52
	SMR	-	-	10	29
	Q1	-	-	9	2
	Median	-	-	10	47
2030	Q3	-	-	11	55
	REF	-	1	10	52
	SMR	-	1	10	52
	Q1	-	-	9	43
2035	Median	-	-	10	50
	Q3	-	1	12	57
	REF	-	17	10	53
	SMR	-	17	10	53
2040	Q1	-	-	9	42
	Median	-	5	11	51
	Q3	-	16	33	58
	REF	-	16	23	54
2045	SMR	-	16	10	54
	Q1	-	-	10	41
	Median	-	12	26	51
	Q3	8	16	68	60
2050	REF	40	16	42	54
	SMR	-	16	11	54
	Q1	-	-	12	42
	Median	-	12	37	52
2050	Q3	35	17	71	60
	REF	39	16	44	55
	SMR	7	16	11	55
	Q1	-	-	11	43
2050	Median	1	13	31	53
	Q3	36	17	66	61

Figure A.1 gives the distribution of the different routes of supply and consumption of gas like methane, hydrogen, ammonia and methanol, resulting from the 1260 samples of the GSA.

Given its lower cost of purchasing than its renewable equivalent (??) and lower global warming potential (GWP) than other fossil fuels (i.e. $gwp_{op,NG} = 0.27 \text{ kt}_{CO_2,\text{eq}}/\text{GWh}$ versus $gwp_{op,LFO} = 0.31 \text{ kt}_{CO_2,\text{eq}}/\text{GWh}$ or $gwp_{op,coal} = 0.40 \text{ kt}_{CO_2,\text{eq}}/\text{GWh}$), fossil NG remains the main source of gas in the system until 2040. Besides bio-hydrolysis as the main consumer of wet biomass to consistently produce gas, e-methane eventually substitutes fossil natural gas by 2045-2050 in order to respect the CO₂-budget for the transition. Its versatility makes gas used by a wide variety of technologies in the different sectors. Initially, in 2020, decentralised gas boilers, CCGT and industrial gas boilers represent the biggest consumers of gas with 39%, 21% and 16% of the total consumption, respectively. Progressively, in line with the rest of the system shifting towards more efficiency in the mid-term, industrial combined heat and power (CHP) represent the lion's share, next to other usages in the transport or LT-heating sectors.

On the contrary, import of fossil-based hydrogen, largely produced from steam-methane-reforming [59], is rarely part of the solution due to the emissions related to the consumption of natural gas. E-hydrogen is the consistent source of hydrogen in the system, next to local production (i.e. steam-methane-reforming, electrolysis or ammonia-cracking) in some rare cases where low industrial EUD coincides with more abundant electricity from SMR or PV. In terms of consumption, fuel cell (FC)-trucks are the more consistent player. FC-cars are also at stake but in specific cases where their CAPEX and the CAPEX of electric vehicles are in the bottom and the top of their respective uncertainty range.

Becoming cheaper than its fossil equivalent at early stages of the transition (i.e. from 2030 onward), e-ammonia is the exclusive stream of ammonia in the system, except rare cases. Then, on top of its consistent NED, the largest consumption of ammonia is CCGT as flexible power generation units, to substitute their e-methane equivalents that have a higher levelised cost of energy (LCOE) (??).

Similarly to ammonia, on top of local production in rare cases, e-methanol is the key source for methanol. Besides its own NED, methanol is mostly consumed to produce HVC via the methanol-to-olefins (MTO) process instead of naphtha-cracking, in order to respect to CO₂-budget for the transition.

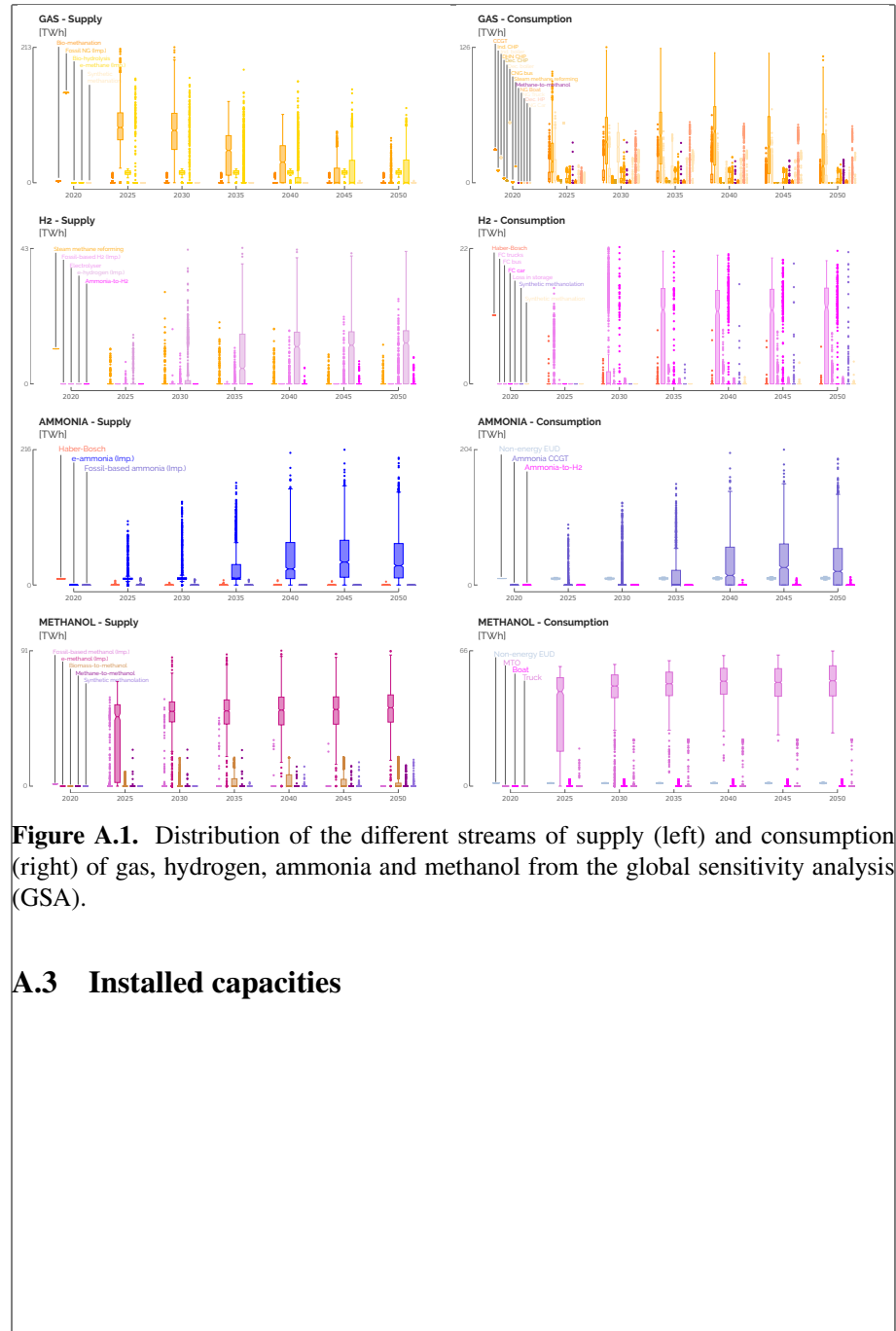


Figure A.1. Distribution of the different streams of supply (left) and consumption (right) of gas, hydrogen, ammonia and methanol from the global sensitivity analysis (GSA).

A.3 Installed capacities

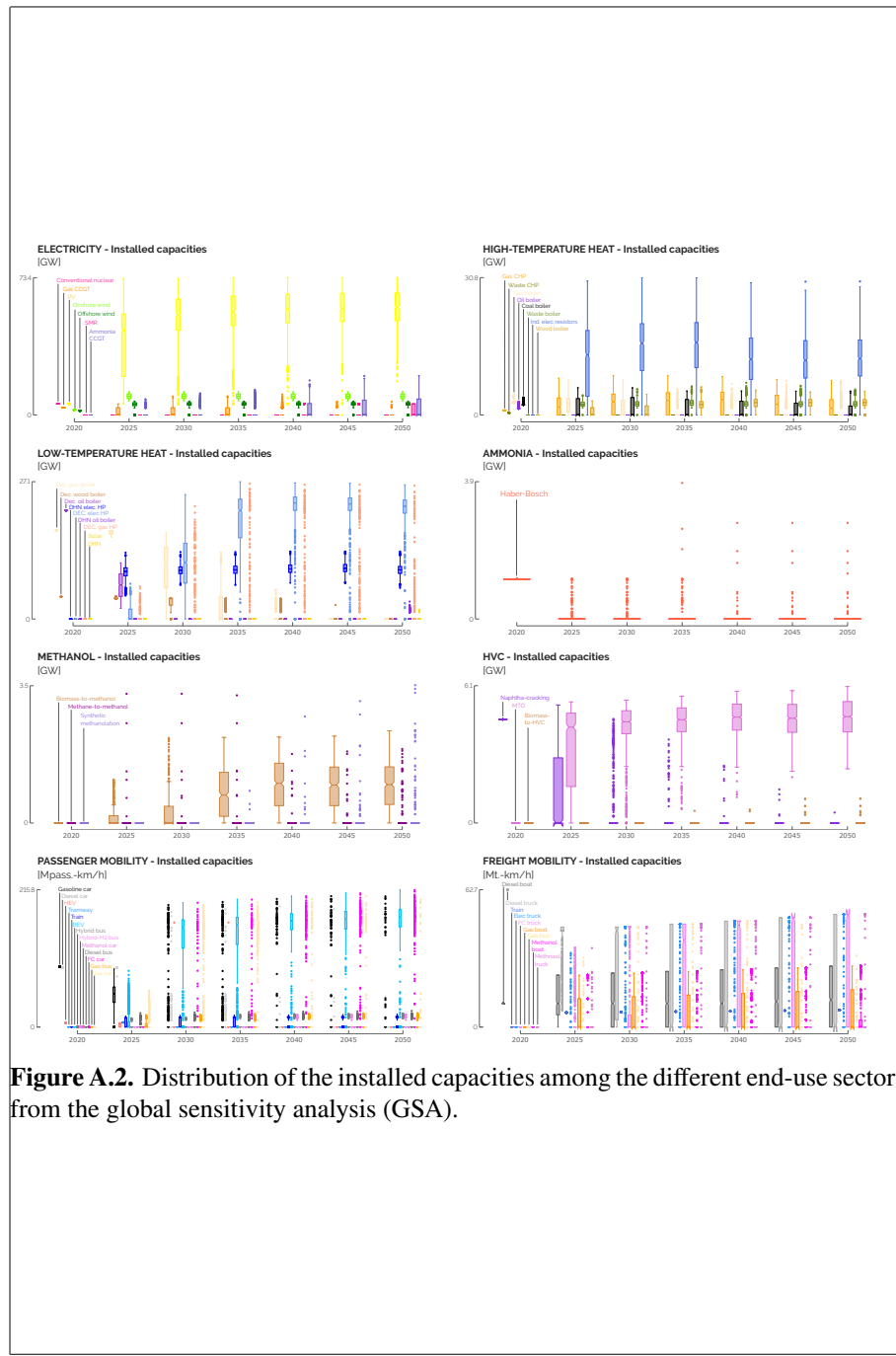


Figure A.2. Distribution of the installed capacities among the different end-use sectors from the global sensitivity analysis (GSA).